

**Ethane dehydrogenation on pristine and AlO_x decorated Pt stepped surfaces**

Journal:	<i>Catalysis Science & Technology</i>
Manuscript ID	CY-ART-02-2018-000398.R1
Article Type:	Paper
Date Submitted by the Author:	15-Mar-2018
Complete List of Authors:	Peng, Guo; University of Wisconsin - Madison, Chemical and Biological Engineering Gerceker, Duygu; University of Wisconsin-Madison, Chemical and Biological Engineering Kumbhalkar, Mrunmayi; University of Wisconsin, Chemical and Biological Engineering Dumesic, James; University of Wisconsin, Chemical and Biological Engineering Mavrikakis, Manos ; University fo Wisconsin - Madison,

Ethane dehydrogenation on pristine and AlO_x decorated Pt stepped surfaces

Guowen Peng¹, Duygu Gerceker¹, Mrunmayi Kumbhalkar¹, James A. Dumesic¹, and Manos Mavrikakis^{1*}

¹*Department of Chemical and Biological Engineering, University of Wisconsin-Madison, Madison, WI 53706, USA*

Abstract

Ethane dehydrogenation on pristine and AlO_x decorated Pt surfaces was studied using density functional theory (DFT) calculations and reaction kinetics experiments. Following the study of adsorption of fourteen distinct C₂H_x and CH_x species, the whole reaction network for ethane dehydrogenation on the terrace and the step of the pristine Pt(433) surface was systematically analyzed using DFT. We show that the under-coordinated step edge sites bind C₂H_x and CH_x species more strongly than terrace sites. These under-coordinated step sites facilitate deep dehydrogenation, resulting in accumulation of coke precursors on the surface and catalyst deactivation. We demonstrate that by decorating the step with AlO_x species the step edge sites can be blocked, leading to substantial suppression of deep dehydrogenation and coke formation. These findings were corroborated by reaction kinetics experiments where a four-fold enhancement of the turnover frequency for ethylene formation was measured on 10-cycle atomic layer deposited (ALD) alumina overcoated Pt/γ-Al₂O₃ catalyst compared to Pt/γ-Al₂O₃ without decoration with ALD-alumina. Our results suggest that AlO_x decorated Pt is a promising catalyst for alkane dehydrogenation and could have applications, including in endothermic cooling in hypersonic flights.

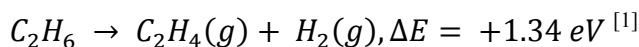
Keywords: density functional theory, ethane dehydrogenation, atomic layer deposition, coke deposition, ethylene

*E-mail: manos@engr.wisc.edu

1. Introduction

Alkane dehydrogenation is an important chemical process in the chemical industry. For example, dehydrogenation of small alkanes can produce light alkenes, such as ethylene, propene, and butene, all important chemicals and platform molecules.

Alkane dehydrogenation reactions are endothermic processes, for example,



In one possible application of these reactions, the heat needed to drive them could be absorbed from the engine and other vehicle components in hypersonic flights, where alkanes are used as the fuel. As a result, endothermic dehydrogenation reactions can, in principle, be used to cool the engine and other vehicle components in hypersonic flights.

Pt group metals are suitable catalysts for alkane dehydrogenation. Extensive experimental^[2–10] and theoretical^[11–20] work has been carried out to study adsorption and reactions of C₂ hydrocarbon species over Pt catalysts. For example, Sinfelt et al. studied the kinetics of ethane hydrogenolysis to methane and reported that the rate of hydrogenolysis is first order in ethane pressure and decreases with increasing hydrogen pressure.^[2,3] Dumesic and co-workers conducted thorough experimental and theoretical studies on ethane hydrogenolysis,^[7,8] stability and reactivity of C₂H_x species^[13,20] over Pt catalysts. They found that the step edge of Pt(211) binds C₂H_x species more strongly than Pt(111) and the primary pathways for ethane hydrogenolysis on Pt involve highly hydrogenated species. Rosch and co-workers^[17], using density functional theory (DFT), studied ethylidyne formation from ethylene and discussed three mechanisms of ethylidyne formation; via vinyl and ethylidene, vinyl and vinylidene and via ethyl and ethylidene on Pt(111). Chen and Vlachos performed a DFT study on hydrogenation of ethylene and dehydrogenation and hydrogenolysis of ethane on Pt(111) and Pt(211).^[18] Further, using DFT, Lu et al. studied the conversion of acetylene to ethylidyne on Pt(111) and proposed a three-step reaction mechanism via vinyl and vinylidene intermediates.^[19]

On Pt catalysts, alkene dehydrogenation to alkynes and C—C bond cracking may also occur. This dehydrogenation generates coke precursors and leads to carbon deposition and deactivation of the catalysts.^[21–23] To mitigate coke formation in alkane dehydrogenation, improve catalyst activity, and achieve better selectivity to alkene production, it has been suggested to alloy Pt with Sn^[24–29] and to co-feed hydrogen^[30,31] with alkanes.

Another approach to prevent coke formation is to cover the catalyst surface with oxide overcoats synthesized with precise thickness control by means of atomic layer deposition (ALD). Stair and co-workers showed that atomic layer deposited (ALD) alumina on Pd/γ-Al₂O₃ reduces catalyst deactivation by coking and sintering for the oxidative dehydrogenation of ethane. In their studies, 45 cycles of ALD alumina overcoated Pd/γ-Al₂O₃ catalysts were probed with diffuse reflectance infrared spectra using CO as a probe molecule. They observed that following the application of this ALD Al₂O₃ coating and calcination of the catalyst at 773 K, the intensities of the CO IR features associated with adsorption on edge and corner Pd atoms were significantly lower than the intensities of the features due CO adsorption on facet planes, indicating that the Al₂O₃ overcoating preferentially decorated the low-coordinated Pd sites.^[32] Similarly, for methanol decomposition, ALD alumina overcoated Pd catalysts demonstrated

enhanced catalytic activity as the overcoat prevents the loss of active surface area during the reaction. Infrared spectroscopy of CO chemisorption on samples overcoated by ALD with alumina revealed that the first cycles of Al_2O_3 deposited preferentially onto the low-coordination sites rather than uniformly covering the particles.^[33] Further, alumina coated Ni nanoparticles were found to be highly resistant to coke deposition and sintering for dry reforming of methane.^[34] Recently, it has been shown that atomic layer deposition (ALD) of an alumina overcoat stabilizes Cu-based catalysts for liquid-phase catalytic reactions. The stability enhancement was attributed to selective armoring of under-coordinated copper atoms on the Cu nanoparticle surface by alumina species. The relative intensities of the bands for CO adsorption on terrace sites and highly under-coordinated copper sites showed that 45 ALD cycles of alumina overcoated on $\text{Cu}/\gamma\text{-Al}_2\text{O}_3$ covered the under-coordinated sites.^[35]

By analogy, one would expect alumina-overcoated Pt catalysts may have better activity and selectivity for alkane dehydrogenation. Considering that the under-coordinated edge sites of Pt nanoparticles bind hydrocarbon species more strongly than Pt terrace sites and thereby could catalyze deep dehydrogenation to form coke precursors, the selectivity of Pt catalysts could be improved if the highly reactive edge sites were blocked by alumina species. A comparative study on microscopic mechanisms of alkane dehydrogenation on pristine and alumina-overcoated Pt would therefore provide useful insights for designing improved catalysts for alkane dehydrogenation.

Here, we report a systematic study on ethane dehydrogenation on pristine and AlO_x decorated Pt(433) stepped surfaces by using DFT calculations in combination with reaction kinetic experiments. We study the adsorption of different C_2H_x and CH_x species on the terrace and step sites and systematically investigate 29 elementary steps for ethane dehydrogenation and cracking. We show that on pristine Pt(433), the under-coordinated step sites accelerate dehydrogenation and lead to formation of coke precursors. We further demonstrate how coke formation can be mitigated on AlO_x -decorated Pt catalysts. The results of our reaction kinetic experiments on ethane dehydrogenation on $\text{Pt}/\gamma\text{-Al}_2\text{O}_3$ and on ALD alumina-overcoated $\text{Pt}/\gamma\text{-Al}_2\text{O}_3$ catalysts show that a 10-cycle ALD/ $\text{Pt}/\gamma\text{-Al}_2\text{O}_3$ catalyst exhibits 4 times higher ethylene turnover frequency (TOF) compared to $\text{Pt}/\gamma\text{-Al}_2\text{O}_3$, in agreement with our DFT predictions. Our results suggest that AlO_x -decorated Pt is a promising catalyst for improved alkane dehydrogenation and thereby could have applications in endothermic fuel cooling in hypersonic flights.

2. Methods

2.1 Computational

All calculations were performed using the Vienna ab-initio Simulation Package (VASP) code based on planewave DFT.^[36,37] The projector augmented wave (PAW) potentials^[38,39] were used for describing

the electron-ion interactions, and the generalized gradient approximation (GGA–PW91)^[40] was used for the exchange-correlation functional. The electron wave function was expanded using plane waves with an energy cutoff of 400 eV. The Pt(433) stepped surface was modeled by a slab of 21 atomic layers in a (1×3) surface unit cell, which has 7-atom wide (111) terrace and 3-atom wide step. Therefore, the surface model provided sufficient numbers of distinct terrace and step edge sites for adsorption, diffusion and reaction of intermediates. A vacuum layer of more than 10 Å was used to separate the slab from its image in the z-direction. The Brillouin zone was sampled using a (1×2×1) k-point mesh based on the Monkhorst-Pack scheme.^[41] The bottom-most 7 layers were fixed during relaxation. All structures were fully relaxed until the Hellmann-Feynman forces acting on the atoms were smaller than 0.05 eV/Å. The climbing image nudged elastic band (CI-NEB) method was used to calculate the activation energy barriers for the individual elementary steps.^[42] Transition states were verified by calculating the Hessian matrix with the finite difference approach and identifying a single imaginary frequency.^[43] The binding energy (BE) for an adsorbate is defined as $BE = E_{\text{ads}} - E_{\text{clean}} - E_{\text{gas}}$, where E_{ads} , E_{clean} , and E_{gas} are the calculated total energies of the slab with the adsorbate on it, the clean slab, and the adsorbate species in the gas phase, respectively.

The Gibbs free energy was calculated by eqn. (1).

$$G(T) = H(T) - TS(T), \quad (1)$$

where H is the enthalpy, T is the temperature, and S is the entropy. To calculate the entropy of species vibrational, translational and rotational contributions were summed together (eqn. (2))

$$S = S_{\text{vib}} + S_{\text{trans}}^{3D} + S_{\text{rot}}, \quad (2)$$

For an adsorbed intermediate, the translational and rotational modes were replaced by vibrational modes corresponding to frustrated translation and rotation on the surface. The vibrational entropy was obtained by eqn. (3)^[44]

$$S_{\text{vib}} = R \sum_i^{\text{no. of modes}} \left(\frac{x_i}{e^{x_i} - 1} - \ln(1 - e^{-x_i}) \right), \quad (3)$$

Where $x_i = \frac{hc}{k_B T} \frac{1}{\lambda_i}$, R is the ideal gas constant, h is the Planck constant, c is the speed of light, k_B is Boltzmann constant and λ_i is the vibrational wavenumber of the i^{th} mode.

For gas phase molecules, the translational entropy was calculated assuming 3D translational freedom while rotational entropy was calculated based on the moments of inertia. The entropy contributions due to 3D translation and rotation are given by eqns. (4) and (5)

$$S_{trans}^{3D} = R \left\{ \ln \left[\left(\frac{2\pi m k_B T}{h^2} \right)^{3/2} \frac{k_B T}{P} \right] + 2.5 \right\}, \quad (4)$$

$$S_{rot} (linear) = R \left\{ \ln \left[\frac{8\pi^2 I_{max} k_B T}{s_{number} h^2} \right] + 1.5 \right\}, \quad (5a)$$

$$S_{rot}(non-linear) = R \left\{ \ln \left[\frac{8\pi^2 (8\pi^3 \prod_i I_i)^{1/2} (k_B T)^{3/2}}{s_{number} h^3} \right] + 1.5 \right\} \quad (5b)$$

respectively, P is the pressure, I_i is the distinguishable principal moments of inertia for a non-linear molecule, I_{max} is principal moment of inertia of a linear molecule along its molecular axis, and s_{number} is the symmetry number of the molecule.

Temperature dependence of the enthalpy is given by eqn. (6)

$$H(T) = H(T = 0 K) + \Delta H_{vib}(T) + \Delta H(T - 0 K), \quad (6)$$

where, the first term is the total energy of the system at 0 K calculated by DFT and $\Delta H_{vib}(T)$ accounts for the vibrational contribution to the enthalpy which was calculated by eqn. (7)

$$H = \sum_i^{no.of\ modes} \left(\frac{1}{2} \frac{hc}{\lambda_i} + \frac{\frac{hc}{\lambda_i}}{e^{\frac{hc}{k_B T}} - 1} \right) \quad (7)$$

The last term denotes the temperature contribution to the enthalpy change. Calculated entropies of the species were used to derive Shomate parameters which subsequently provided heat capacity values of the species and temperature contribution to the enthalpy change.^[44]

2.2 Experimental

Catalyst preparation and characterization: Platinum was dispersed onto γ -Al₂O₃ (Strem Chemicals Inc, 210 m² g⁻¹) by incipient wetness impregnation, using tetra-ammine platinum(II) nitrate (Sigma-Aldrich, 99%) as the metal precursor to synthesize a 1wt% Pt/ γ -Al₂O₃ catalyst. After drying the mixture overnight in an oven at 383 K, the catalyst was calcined in flowing air at 673 K for 2 h. The sample was cooled to ambient temperature and then reduced at 773 K for 2 h (1 K/min temperature ramp) under flowing hydrogen. The sample was again cooled to ambient temperature and passivated in flowing 1% O₂/Ar for 1 h.

To prepare the alumina-overcoated Pt catalyst, the parent Pt/ γ -Al₂O₃ was overcoated with alumina using ALD. ALD is a self-limiting growth process that gives highly conformal coatings.^[45,46] Amorphous alumina overcoat was deposited by 10 cycles of alternate exposure to trimethyl-aluminum and water at 473 K in a fluidized bed reactor described elsewhere.^[47] Henceforth, the parent and alumina-overcoated catalysts will be termed as non-overcoated Pt/ γ -Al₂O₃ and 10cALD/Pt/ γ -Al₂O₃, respectively. The number of surface Pt atoms (Pt_s) was calculated using the volumetric uptake of CO at 308 K (Micromeritics, ASAP 2020C analyzer). Amount of coke deposition on the spent catalysts was determined by thermogravimetric analysis (TGA) using a TGA analyzer (TA Instruments Q500 analyzer).

Reaction kinetics studies: Reaction kinetics studies of ethane conversion were conducted in a continuous fixed-bed stainless-steel down flow reactor operated at atmospheric pressure. Alkane dehydrogenation is limited by chemical equilibrium and for lighter paraffins, high temperature is required for significant conversion. The experiments were performed at 873 K with helium (Airgas) as the carrier gas. Prior to collecting the reaction kinetics data, the catalyst was reduced *in situ* at 773 K for 1 h. Initial ethane reactivities were measured using a feed mixture containing 12.5 Torr ethane (Airgas), 0-50 Torr hydrogen (Airgas) and balance helium for a total pressure of 1 atm. Reactants and products were analyzed using a gas chromatographer (Shimadzu Corp., GC-2014) equipped with a Rt®-Alumina BOND/MAPD capillary column and a flame ionization detector. To compare the ethylene formation over the catalysts, the turnover frequency was calculated based on the number of surface platinum atoms determined by CO chemisorption. We assumed a stoichiometry of one CO molecule per surface platinum atom. The non-overcoated Pt/ γ -Al₂O₃ and 10cALD/Pt/ γ -Al₂O₃ catalysts had 29 $\mu\text{mol g}^{-1}$ and 3 $\mu\text{mol g}^{-1}$ of surface Pt sites, respectively. Overcoating with alumina decreases the extent of CO adsorption on Pt/ γ -Al₂O₃ indicating that alumina overcoat is covering a fraction of the exposed Pt atoms. The reusability of a catalyst for endothermic cooling was determined by performing a set of successive reaction and regeneration experiments on the catalyst. After *in situ* reduction of a fresh catalyst at 773 K, the reactor was heated to 873 K in helium and reaction was carried out at atmospheric pressure with 12.5 Torr ethane, 0 Torr hydrogen and balance helium. At these reaction conditions, the equilibrium conversion of ethane dehydrogenation to ethylene is 72%, therefore, during the experiment ethane conversion was maintained at less than 20% of this value. Upon completion of an experiment, the reactor was purged with helium and simultaneously cooled to ambient temperature. The spent catalyst was then regenerated by calcining in flowing air at 673 K for 1 h. The catalyst bed was again purged with helium, reduced under flowing hydrogen at 773 K and subsequently exposed to the reactant mixture at the aforementioned experimental conditions.

Quantification of the deposited coke on the catalysts was accomplished by utilizing thermogravimetric analysis (TGA). The experiments performed to collect samples for TGA were conducted in the following manner. To ensure a flow of equilibrated mixture of ethane, ethylene and hydrogen through the catalyst under evaluation, a dual bed reactor system was used, consisting of a pre-bed with lesser deactivating catalyst e.g. Pt/Sn/K-L-Zeolite. Following the reaction with 50 Torr hydrogen co-feed, the reactor was cooled to ambient conditions under flowing He and the catalyst was retrieved by cutting the reactor. It was assumed that the weight loss during thermogravimetric analysis is solely due the removal of surface deposited coke via CO₂ formation.

3. Results and Discussion

3.1 Adsorption of C₂H_x and CH_x species on Pt(433)

We first studied adsorption of C₂H_x species for ethane dehydrogenation on the terrace of Pt(433)-(1x3). Shown in Fig. 1(a) – (j) are cross-section and the top views of the minimum energy structures of the most favorable adsorption sites for different C₂H_x species. Ethane (C₂H₆) binds weakly to the Pt terrace with a binding energy of -0.05 eV and at a distance of 3.1 Å above the surface. Ethyl (C₂H₅) prefers a top site, with a binding energy of -2.09 eV and a C—Pt bond length of 2.09 Å. For ethylene (C₂H₄), the di-σ bonded configuration is the most stable, with a binding energy of -1.34 eV; the length of the two C—Pt bonds is 2.11 Å. The C—C bond in adsorbed ethylene (C₂H₄) is elongated to 1.49 Å, from its value of 1.33 Å in the gas phase. The π-bonded configuration of ethylene (C₂H₄), where both C atoms bind to the same Pt atom is less stable, with a binding energy of -0.95 eV. Vinyl (CH₂-CH) prefers a top-bridge site: the CH₂ moiety binds atop Pt, with a C—Pt bond length of 2.09 Å; the CH moiety in vinyl (CH₂-CH) sits above a bridge site, with a length of 2.07 Å for the two C—Pt bonds. The calculated binding energy is -3.50 eV. The most favorable site for acetylene (C₂H₂) is a bridge-bridge site with a binding energy of -2.57 eV. In the bridge-bridge configuration, each CH moiety binds on an adjacent bridge site; one shorter C—Pt bond (2.00 Å) and one longer C—Pt bond (2.21 Å, with a single Pt binding with two C atoms) are formed. The C—C bond length is elongated to 1.39 Å compared to 1.21 Å in the gas phase C₂H₂. Ethylidene (CH₃-CH) prefers to bind to a bridge site (via CH) with a binding energy of -4.17 eV and a C—Pt bond length of 2.07 Å. The C-C bond in adsorbed ethylidene (CH₃-CH) is 1.50 Å. We note that on the terrace, the adsorbed ethylidene (CH₃-CH) is only 0.27 eV less stable than its isomer adsorbed ethylene (C₂H₄); while in the gas phase, ethylidene (CH₃-CH) is 3.10 eV less stable than ethylene (C₂H₄). Ethylidyne (CH₃-C) prefers a threefold hollow site (via C) and three C—Pt bonds are formed (bond length of 2.02 Å). The binding energy is -6.24 eV and the C-C bond in that state is 1.49 Å. Vinylidene (CH₂-C) prefers to adsorb at a top-fcc site, with a binding energy of -4.71 eV. Ethynyl (CH-C) prefers a bridge-hollow (fcc or hcp) site with a binding energy of -5.19 eV

and a C-C bond length of 1.41 Å. The CC dimer prefers to bind to adjacent hollow sites (fcc and hcp), with a binding energy of -6.68 eV and a C-C bond length of 1.36 Å. The binding geometries and binding energies of all C_2H_x species are summarized in Table 1. Our results are in agreement with the literature.^[17,18,20] From the binding geometries of C_2H_x , we note that structures maintaining four-coordinated C are the most favorable. This behavior is also true for adsorption of CH_x species on the terrace. The calculated most stable binding sites and the respective binding energies for CH_x species are provided in Table 1. CH_3 , CH_2 , CH , and C prefers atop, bridge, fcc hollow, and fcc hollow sites, with a binding energy of -2.22, -4.32, -6.96, -7.34 eV, respectively. H prefers to adsorb to either the top or fcc site with a calculated energy of -2.78 eV.

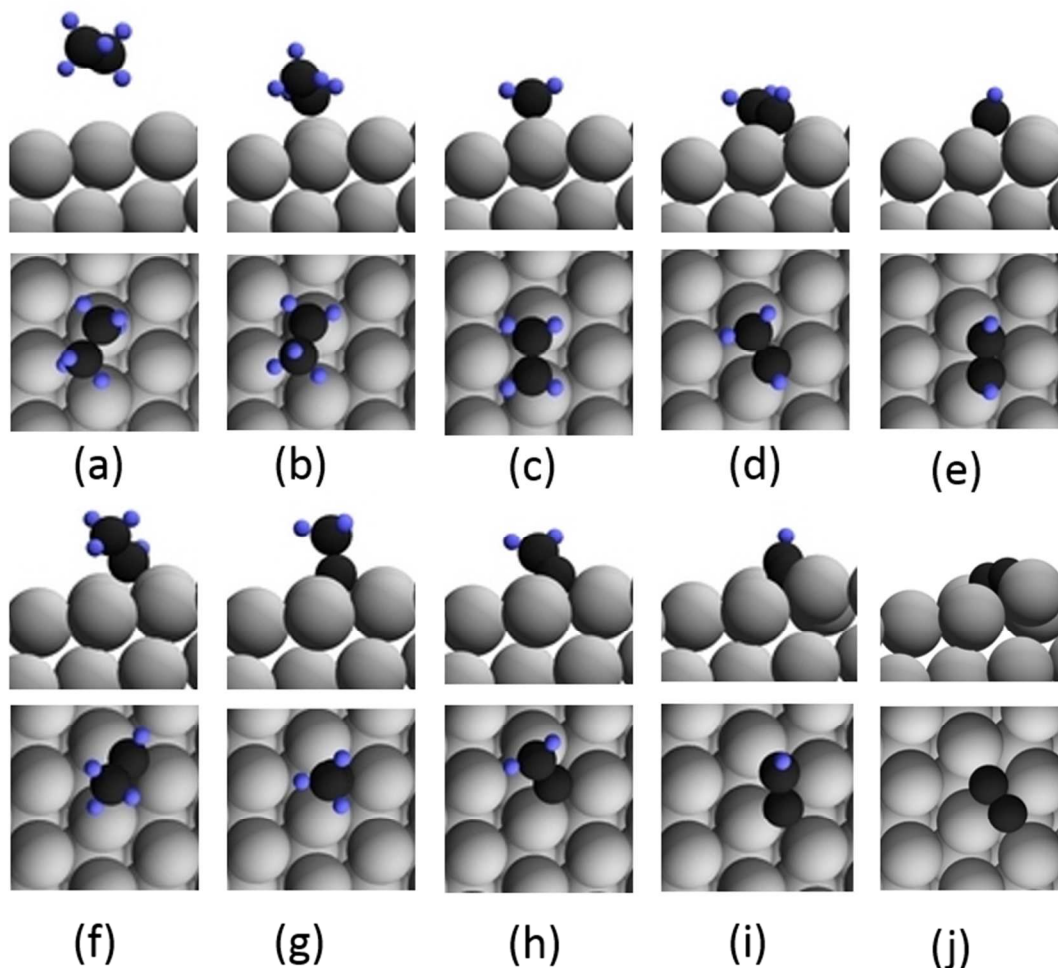


Figure 1. Cross-section and top views of optimized structures for C_2H_x species on the terrace of Pt(433). (a) ethane C_2H_6 , (b) ethyl C_2H_5 , (c) ethylene C_2H_4 , (d) vinyl CH_2-CH , (e) acetylene C_2H_2 , (f) ethylidene CH_3-CH , (g) ethylidyne CH_3-C , (h) vinylidene CH_2-C , (i) ethynyl $CH-C$, and (j) CC. Gray, black and blue spheres denote Pt, C, and H atoms, respectively.

Table 1. Preferred binding geometries and binding energies (BE, in eV) of C_2H_x and CH_x species on pristine and Al_6O_{11} decorated Pt(433) surfaces. Phys stands for physisorbed, with no site specificity.

Species	Pt(433) Terrace		Pt(433) Step		Al_6O_{11} decorated Pt(433)	
	Site	BE	Site	BE	Site	BE
C_2H_6	phys	-0.05	phys	-0.13	phys	-0.07
C_2H_5	top	-2.09	top	-2.26	top	-2.12
C_2H_4	di- σ	-1.34	di- σ	-1.73	di- σ	-1.35
CH_2-CH	top-bri	-3.50	top-bri	-3.94	top-bri	-3.46
C_2H_2	bri-bri	-2.57	bri-bri	-2.93	bri-bri	-2.50
CH_3-CH	bri	-4.17	bri	-4.72	bri	-4.18
CH_3-C	fcc	-6.24	hcp	-6.21	fcc	-6.23
CH_2-C	top-fcc	-4.71	top-hcp	-4.75	top-fcc	-4.61
$CH-C$	bri-hollow	-5.19	bri-hcp	-5.43	bri-hcp	-4.98
CC	fcc-hcp	-6.68	fcc-hcp	-7.23	fcc-hcp	-6.49
CH_3	top	-2.22	top	-2.43	top	-2.24
CH_2	bri	-4.32	bri	-4.91	bri	-4.31
CH	fcc	-6.96	hcp	-6.93	fcc	-6.94
C	fcc	-7.34	hcp	-7.44	fcc	-7.25
H	top/fcc	-2.78	bri	-3.03	top/fcc	-2.79

We next studied the adsorption of C_2H_x species at the step edge of Pt(433). Figure 2 illustrates the most stable atomic structures of C_2H_x species adsorbed at the step. The C_2H_x binding preference on the step is similar to that on the terrace, whereby formation of saturated four-coordinated carbon is preferred. The calculated binding energies of C_2H_x species at the step are summarized in Table 1. Ethane (C_2H_6) binds weakly (physisorption), with a calculated binding energy of -0.13 eV. The top site at the step edge binds ethyl (C_2H_5) with -2.26 eV, which is 0.17 eV more strongly than the top site on the terrace. The di- σ bonded ethylene (C_2H_4) at the step edge binds with -1.73 eV, which is 0.39 eV more stable than that on the terrace. The step binds vinyl (CH_2-CH) at the top-bridge site 0.44 eV more stable than the terrace. The binding energy of bridge-bridge bound acetylene (C_2H_2) at the step is -2.93 eV, which is 0.36 eV

more stable than that on the terrace. Similarly, ethylidene ($\text{CH}_3\text{-CH}$) binds 0.55 eV more stable at the step edge than on the terrace. For ethylidyne ($\text{CH}_3\text{-C}$), we found the hcp site near the step edge is nearly as stable as the fcc site on the terrace (ca. -6.20 eV). Vinylidene ($\text{CH}_2\text{-C}$) binds at the step via a top-hcp configuration and is slightly more stable (by 0.04 eV) than on the terrace. CH-C binds on the bridge-hcp site at the step edge and is 0.24 eV more stable than on the terrace. The CC dimer bound at adjacent fcc and hcp hollow sites near the step is also found to be 0.55 eV more stable than on the terrace. For CH_x species, we calculated that CH_3 and CH_2 binds 0.21 and 0.59 eV more strongly at the step edge than on the terrace, respectively; CH prefers the hcp site near the step edge and is nearly as stable as on the fcc site on the terrace. C prefers the hcp site near the step edge and is slightly more stable (by 0.1 eV) than on the terrace. H binds on the bridge site on the step edge and is 0.25 eV more stable than on the terrace. A comparison of the binding energy at the step edge and the terrace presented in Table 1 clearly shows that the under-coordinated step sites bind species more strongly than terrace sites.

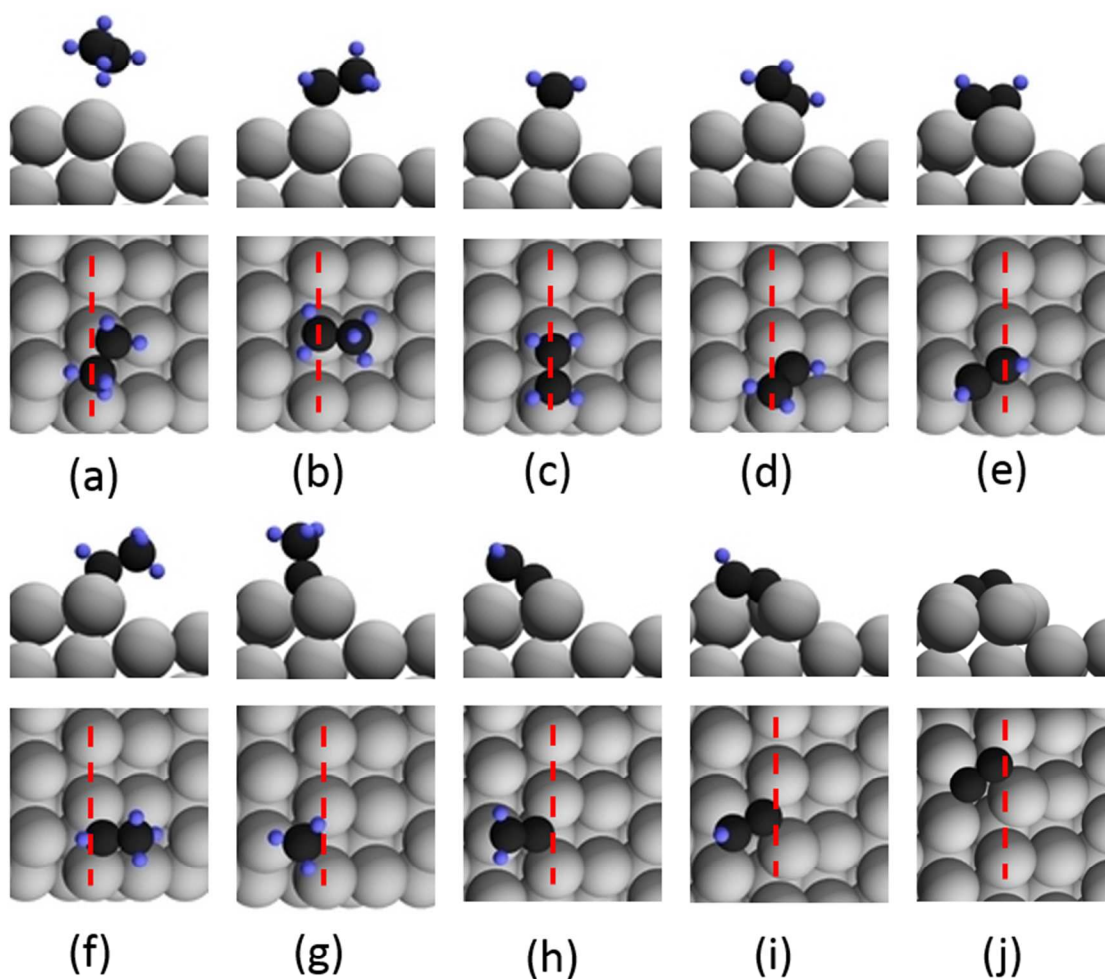


Figure 2. Cross-section and top views of optimized structures for C_2H_x species at the step of Pt(433). (a) ethane C_2H_6 , (b) ethyl C_2H_5 , (c) ethylene C_2H_4 , (d) vinyl CH_2-CH , (e) acetylene C_2H_2 , (f) ethylidene CH_3-CH , (g) ethylidyne CH_3-C , (h) vinylidene CH_2-C , (i) ethynyl $CH-C$, and (j) CC. Gray, black and blue spheres denote Pt, C, and H atoms, respectively. The step edge is highlighted with a red dashed line.

3.2. Ethane dehydrogenation on Pt(433) terrace

Having studied the adsorption of C_2H_x and CH_x species on the terrace and step of Pt(433), we now turn our attention to investigate the activation energy barriers for ethane dehydrogenation on the terrace, followed by the study of ethane dehydrogenation at the step edge. Barriers for C—C bond breaking steps are also discussed.

Elementary steps of ethane dehydrogenation on the terrace

(1) *Ethane (C_2H_6) to ethyl (C_2H_5).* The initial state of the first hydrogen abstraction step involves the physisorbed ethane (C_2H_6), whereas the final state has ethyl (C_2H_5) bound on a top Pt site and a co-adsorbed H atom in the second-nearest neighboring fcc site. During the reaction, ethane (C_2H_6) moves toward the surface. At the transition state, the C—Pt distance reaches 2.30 Å; the reactive H binds atop Pt (H—Pt length is 1.65 Å); and the C—H bond elongates to 1.52 Å. Next, in the reaction coordinate, the C—H bond breaks and H reaches a Pt bridge site before it settles to the final hollow site. On the terrace, ethane (C_2H_6) dehydrogenation to ethyl (C_2H_5) is exothermic with a reaction energy of -0.16 eV and an activation energy barrier of 0.65 eV.

(2) *Ethyl (C_2H_5) to ethylene (C_2H_4).* To remove a H from ethyl (C_2H_5) towards the formation of di- σ bonded ethylene (C_2H_4), the CH_3 end of ethyl (C_2H_5) bound atop Pt moves close to the adjacent Pt. At the transition state, the C atom of CH_3 binds to the adjacent Pt atom with a distance of 2.36 Å; the reactive H makes a bond with the same adjacent Pt atom (H—Pt: 1.68 Å) and the H—C bond is elongated to 1.50 Å. This elongated H—C bond is subsequently broken with H located at a Pt bridge site before it further diffuses to the most stable fcc site at the second-nearest neighbor. This dehydrogenation is exothermic (-0.22 eV) and has an activation energy barrier of 0.71 eV.

(3) *Ethylene (C_2H_4) to vinyl (CH_2-CH).* Ethylene (C_2H_4) starts by rotating around one CH_2 end to bring the other C to the nearest bridge site to form vinyl (CH_2-CH). At the transition state, two C—Pt bonds are formed with lengths of 2.19 and 2.09 Å; the reactive H sits atop of Pt with a H—Pt bond length of 1.63 Å, whereas the H—C bond is elongated to 1.50 Å. The H—C bond is broken next, and H moves to the bridge before diffusing to the fcc site at the second-nearest neighbor. This step is endothermic (by 0.09 eV) and has an activation energy barrier of 0.78 eV.

(4) *Vinyl (CH_2-CH) to acetylene (C_2H_2)*. This H abstraction step is 0.08 eV endothermic with an activation energy barrier of 0.89 eV. At the transition state, the reactive H is at an off-top site with a H—Pt distance of 1.64 Å; the reactive C atom moves to the bridge site and a second C—Pt with a length of 2.21 Å is formed.

(5) *Ethyl (C_2H_5) to ethylidene (CH_3-CH)*. When an H is abstracted from the CH_2 end of ethyl (C_2H_5), ethylidene (CH_3-CH) is formed. Our calculations suggest that ethyl (C_2H_5) is dehydrogenated to ethylidene (CH_3-CH) bound atop of Pt first, with an activation energy barrier of 0.81 eV. At the transition state, the H—C bond is elongated to 1.48 Å and H is at a distance of 1.64 Å from a neighboring Pt atom. Compared with the exothermic dehydrogenation of ethyl (C_2H_5) to ethylene (C_2H_4), ethyl (C_2H_5) dehydrogenation to ethylidene (CH_3-CH) is endothermic with a reaction energy of 0.04 eV and an activation energy barrier of 0.81 eV, which is higher than that from ethyl (C_2H_5) to ethylene (C_2H_4) (0.71 eV), suggesting that ethylene (C_2H_4) is the main product of ethyl (C_2H_5) dehydrogenation on the terrace of Pt(433).

(6) *Vinyl (CH_2-CH) to ethylidene (CH_3-CH)*. Considering the fact that the formation of ethylidene (CH_3-CH) from ethyl (C_2H_5) dehydrogenation is both thermodynamically and energetically less favorable than the formation of ethylene, we also studied hydrogenation of vinyl (CH_2-CH) to ethylidene (CH_3-CH). This hydrogenation step is slightly endothermic with a reaction energy of 0.15 eV. At the transition state, the H is at the off-top Pt site with a H—Pt distance of 1.60 Å; the distance between H and C (of CH_2) is 1.56 Å. The H moves further close to C to form the H—C bond, whereas the H—Pt bond is being broken. The activation energy barrier is 0.80 eV. If we take the energies of adsorbed H and vinyl at infinite separation as a reference, the effective barrier is 0.89 eV. This value is comparable with the barrier of vinyl (CH_2-CH) dehydrogenation to acetylene (C_2H_2), i.e., step (4) as discussed earlier.

(7) *Ethylidene (CH_3-CH) to ethylidyne (CH_3-C)*. This step is exothermic by -0.70 eV, primarily due to the stability of the adsorbed ethylidyne (CH_3-C) at the hollow site. The activation energy barrier is 0.23 eV. During the reaction, the reactive C moves from a bridge site to a hollow site. At the transition state, the H—Pt distance is 1.76 Å and the H—C distance is 1.24 Å. Subsequently, the H—C bond breaks and the H settles at the adjacent hollow site.

(8) *Ethylidyne (CH_3-C) to vinylidene (CH_2-C)*. The dehydrogenation of ethylidyne (CH_3-C) to vinylidene (CH_2-C) is an endothermic and highly activated process. The reaction energy and activation energy barrier is 0.40 and 1.27 eV, respectively. During the course of the reaction, CH_3-C bends toward the surface to bring CH_3 close to a top site of Pt. At the transition state, the H is at the Pt top site with a H—Pt distance of 1.62 Å; the H—C distance is 1.66 Å; and the distance between the CH_2 group and the Pt atom to which H is bound is 2.35 Å.

(9) *Vinyl (CH₂-CH) to vinylidene (CH₂-C)*. The dehydrogenation of vinyl (CH₂-CH) to vinylidene (CH₂-C) is exothermic by 0.13 eV, with an activation energy barrier of 0.55 eV. During the reaction, the reactive C moves from the bridge site to the three-fold hollow site. At the transition state, the C is on the hollow site and H is on atop Pt site; the H—C and H—Pt distances are 1.43 and 1.65 Å, respectively.

(10) *Vinylidene (CH₂-C) to ethynyl (CH-C)*. This elementary step involves the formation of an intermediate state CH-C at top-fcc site by breaking one C—H bond with a high activation energy barrier of 1.43 eV. At the transition state, the active H binds with a neighboring Pt with a H—Pt distance of 1.66 Å whereas the H—C bond length is 1.74 Å. The intermediate CH-C at top-fcc site transforms to the more stable final state at top-hollow site easily. Vinylidene (CH₂-C) to ethynyl (CH-C) is highly endothermic (0.90 eV).

(11) *Acetylene (C₂H₂) to ethynyl (CH-C)*. This step is endothermic with a reaction energy of 0.69 eV. The reactive C moves from a bridge to the neighboring hollow site. At the transition state, the active H is at an off-top Pt site with a H—Pt distance of 1.64 Å, whereas the H—C bond is elongated to 1.60 Å. The activation energy barrier is 1.28 eV.

(12) *Ethynyl (CH-C) to CC*. The final dehydrogenation step is endothermic (0.93 eV) and highly activated (1.58 eV), and produces a carbon dimer at an fcc-hcp site. At the transition state, one C moves from the bridge site to fcc site; H is at an off-top Pt site with the H—Pt distance at 1.64 Å and the H—C distance at 1.58 Å.

Table 2 summarizes the activation energy barriers and reaction energies for all these 12 key elementary steps. The corresponding values of co-adsorbed species at infinite separation are also included in parentheses. We further calculated three isomerization steps, namely, (13) ethylene (C₂H₄) to ethylidene (CH₃-CH), (14) vinyl (CH₂-CH) to ethylidyne (CH₃-C), and (15) vinylidene (CH₂-C) to acetylene (C₂H₂). The results are also provided in Table 2. All three C₂ isomerization steps (13), (14), and (15) are highly activated, with an activation energy barrier of 2 eV or above.

Table 2. Energy barrier (E_a , in eV) and reaction energy (ΔE , in eV) of elementary steps for ethane dehydrogenation on pristine and Al₆O₁₁ decorated Pt(433) surfaces. Number in parentheses are values for infinite separation in co-adsorbed species.

Elementary Step	Pt(433) Terrace		Pt(433) Step		Al ₆ O ₁₁ decorated Pt(433)	
	E_a	ΔE (ΔE_{inf})	E_a	ΔE (ΔE_{inf})	E_a	ΔE (ΔE_{inf})
1. C ₂ H ₆ → C ₂ H ₅ +H	0.65	-0.16 (-0.23)	0.33	-0.35 (-0.57)	0.69	-0.16 (-0.26)
2. C ₂ H ₅ → C ₂ H ₄ +H	0.71	-0.22 (-0.28)	0.27	-0.64 (-0.76)	0.73	-0.22 (-0.29)
3. C ₂ H ₄ → CH ₂ -CH+H	0.78	0.09 (0.00)	0.42	-0.18 (-0.28)	0.84	0.17 (0.06)

4. $\text{CH}_2\text{-CH} \rightarrow \text{C}_2\text{H}_2 + \text{H}$	0.89	0.08 (-0.05)	1.29	-0.03 (-0.17)	0.95	0.14 (0.01)
5. $\text{C}_2\text{H}_5 \rightarrow \text{CH}_3\text{-CH} + \text{H}$	0.81	0.04 (-0.04)	0.08	-0.62 (-0.67)	0.78	0.17 (-0.02)
6. $\text{CH}_2\text{-CH} + \text{H} \rightarrow \text{CH}_3\text{-CH}$	0.80 (0.89)	0.15 (0.24)	0.97 (1.06)	0.30 (0.39)	0.77 (0.88)	0.10 (0.21)
7. $\text{CH}_3\text{-CH} \rightarrow \text{CH}_3\text{-C} + \text{H}$	0.23	-0.70 (-0.77)	0.73	-0.40 (-0.45)	0.31	-0.67 (-0.76)
8. $\text{CH}_3\text{-C} \rightarrow \text{CH}_2\text{-C} + \text{H}$	1.27	0.40 (0.34)	0.89	0.10 (-0.02)	1.29	0.40 (0.39)
9. $\text{CH}_2\text{-CH} \rightarrow \text{CH}_2\text{-C} + \text{H}$	0.55	-0.13 (-0.19)	0.81	0.08 (-0.04)	0.65	-0.12 (-0.13)
10. $\text{CH}_2\text{-C} \rightarrow \text{CH-C} + \text{H}$	1.43	0.90 (0.79)	1.41	0.37 (0.34)	1.52	1.00 (0.89)
11. $\text{C}_2\text{H}_2 \rightarrow \text{CH-C} + \text{H}$	1.28	0.69 (0.60)	1.49	0.51 (0.47)	1.44	0.85 (0.75)
12. $\text{CH-C} \rightarrow \text{CC} + \text{H}$	1.58	0.93 (0.85)	1.40	0.67 (0.29)	1.61	0.94 (0.82)
13. $\text{C}_2\text{H}_4 \rightarrow \text{CH}_3\text{-CH}$	2.12	0.27	2.24	0.11	2.04	0.26
14. $\text{CH}_2\text{-CH} \rightarrow \text{CH}_3\text{-C}$	2.00	-0.54	2.02	-0.06	1.97	-0.56
15. $\text{CH}_2\text{-C} \rightarrow \text{C}_2\text{H}_2$	2.50	0.18	2.36	-0.14	2.51	0.15

Elementary steps for C—C bond breaking at the terrace of Pt(433)

We then studied C—C bond breaking steps which decompose C_2H_x species into CH_x species. The results are summarized in Table 3, steps 16 to 25. Comparing results in Table 2 and Table 3, we conclude that the C—C bond breaking step is kinetically less favorable than the corresponding dehydrogenation step. C—C bond breaking in ethane (C_2H_6) (step 16) has a barrier of 2.77 eV, which is significantly higher than the barrier (0.65 eV) for ethane dehydrogenation to ethyl (C_2H_5) (step 1). C—C bond breaking in ethyl (C_2H_5) (step 17), has a barrier of 2.01 eV, whereas ethyl's dehydrogenation to ethylene (C_2H_4) (step 2) and ethylidene ($\text{CH}_3\text{-CH}$) (step 5) has a barrier of 0.71 and 0.81 eV, respectively. C—C bond breaking in ethylene (C_2H_4) (step 18) has a barrier of 2.19 eV, as compared to a barrier of 0.78 eV for ethylene dehydrogenation to vinyl ($\text{CH}_2\text{-CH}$) (step 3). C—C bond breaking in ethylidene ($\text{CH}_3\text{-CH}$) (step 19) has a barrier of 1.27 eV, whereas its dehydrogenation to ethylidyne ($\text{CH}_3\text{-C}$) (step 7) is facile (0.23 eV). C—C bond breaking in ethylidyne ($\text{CH}_3\text{-C}$) (step 20) has a barrier of 1.91 eV, versus 1.27 eV for its dehydrogenation to vinylidene ($\text{CH}_2\text{-C}$) (step 8). C—C bond breaking in vinyl ($\text{CH}_2\text{-CH}$) to CH_2 and CH (step 21) is also unfavorable compared to its dehydrogenation to vinylidene ($\text{CH}_2\text{-C}$) (step 9): 1.75 eV energy barrier for C—C bond breaking versus 0.55 eV energy barrier for dehydrogenation. We found that the decomposition of acetylene (C_2H_2) to two CH (step 22) is easier than the corresponding dehydrogenation to ethynyl CH-C (step 11): the C—C bond breaking

has a barrier of 0.99 eV, when the acetylene dehydrogenation has a barrier of 1.28 eV. This comparison indicates that C—C bond breaking may occur at the adsorbed acetylene (C_2H_2) state, which is reminiscent of findings for ethane (C_2H_6) hydrogenolysis on Ir(111).^[48] C—C bond breaking in vinylidene (CH_2-C) to CH_2 and C (step 23) is highly activated (2.51 eV), as compared to vinylidene's dehydrogenation to ethynyl $CH-C$ and H (step 10, 1.43 eV). C—C bond breaking in ethynyl ($CH-C$) to CH and C (step 24, $E_a = 0.96$ eV) is more favorable than the respective dehydrogenation to CC (step 12, $E_a = 1.58$ eV). Finally, breaking of the C-C dimer to two C atoms has a moderate energy barrier of 0.68 eV.

Table 3. Energy barrier (E_a , in eV) and reaction energy (ΔE , in eV) of elementary steps for C—C bond breaking of C_2H_x species, and dehydrogenation of CH_x species on pristine and Al_6O_{11} decorated Pt(433) surfaces. Numbers in parentheses are values for infinite separation in co-adsorbed species.

Elementary Step	Pt(433) Terrace		Pt(433) Step		Al_6O_{11} decorated Pt(433)	
	E_a	$\Delta E(\Delta E_{inf})$	E_a	$\Delta E(\Delta E_{inf})$	E_a	$\Delta E(\Delta E_{inf})$
16. $C_2H_6 \rightarrow CH_3+CH_3$	2.77	-0.01 (-0.12)	1.99	-0.27 (-0.46)	2.76	-0.07 (-0.15)
17. $C_2H_5 \rightarrow CH_3 + CH_2$	2.01	0.26 (0.22)	1.58	-0.25 (-0.40)	2.08	0.33 (0.24)
18. $C_2H_4 \rightarrow CH_2+CH_2$	2.19	0.75 (0.62)	1.53	0.12 (-0.13)	2.27	0.83 (0.68)
19. $CH_3-CH \rightarrow CH_3+CH$	1.27	-0.33 (-0.37)	1.36	0.16 (0.00)	1.31	-0.24 (-0.36)
20. $CH_3-C \rightarrow CH_3+C$	1.91	0.88 (0.82)	1.62	0.66 (0.52)	2.00	0.96 (0.92)
21. $CH_2-CH \rightarrow CH_2+CH$	1.75	0.06 (-0.06)	2.33	0.12 (-0.12)	1.84	0.04 (-0.02)
22. $C_2H_2 \rightarrow CH+CH$	0.99	-0.64 (-0.73)	1.35	0.16 (-0.21)	1.05	-0.43 (-0.66)
23. $CH_2-C \rightarrow CH_2+C$	2.51	0.69 (0.68)	2.23	0.27 (0.04)	2.53	0.76 (0.69)
24. $CH-C \rightarrow CH + C$	0.96	-0.51(-0.74)	1.00	-0.33 (-0.57)	0.96	-0.64 (-0.84)
25. $CC \rightarrow C+C$	0.68	-0.95 (-1.09)	0.93	-0.47 (-0.75)	0.71	-1.03 (-1.10)
26. $CH_4 \rightarrow CH_3+H$	0.68	-0.10 (-0.16)	0.28	-0.51 (-0.59)	0.72	-0.09 (-0.18)
27. $CH_3 \rightarrow CH_2+H$	0.77	0.21 (0.12)	0.13	-0.45 (-0.51)	0.81	0.25 (0.14)
28. $CH_2 \rightarrow CH+H$	0.25	-0.58 (-0.64)	0.69	-0.20 (-0.27)	0.23	-0.53 (-0.63)

29. CH → C+H	1.22	0.56 (0.50)	1.08	0.20 (0.12)	1.32	0.66 (0.57)
--------------	------	-------------	------	-------------	------	-------------

Dehydrogenation of CH_x species on the terrace

As discussed above, C—C bond-breaking in adsorbed acetylene (CH-CH*) and ethynyl (CH-C*) is energetically more favorable than the corresponding dehydrogenation step, indicating that hydrogenolysis to final product methane (CH₄) could take place. For completeness, we therefore calculated the dehydrogenation steps of CH_x species. The results are provided in Table 3. The activation energy barriers for the first, second, third, and fourth dehydrogenation steps of CH_x species (steps 26, 27, 28 and 29) are 0.68, 0.77, 0.25, and 1.22 eV, respectively. Collectively, the reverse of these steps contribute to CH₄ production.

Potential energy diagram of ethane dehydrogenation on the Pt(433) terrace

The potential energy diagram (PED) for ethane dehydrogenation in Fig. 3 (a) was constructed utilizing the energetics of all elementary steps of ethane (C₂H₆) dehydrogenation on the Pt(433) terrace. Note that in the PED, when there is co-adsorbed H, we took the total energy of the co-adsorbed system at infinite separation as a reference energy. These data are given in parentheses in Table 2. Fig. 3(a) shows that the path for ethane (C₂H₆) dehydrogenation to ethylene (C₂H₄) and further to acetylene (C₂H₂) is C₂H₆* → C₂H₅* + H* → C₂H₄* + 2H* → CH-CH₂* + 3H* → C₂H₂* + 4H*. The desorption of adsorbed ethylene (C₂H₄) requires an activation energy barrier of 1.34 eV, whereas ethylene dehydrogenation to vinyl (CH₂-CH) has a barrier of 0.78 eV. Desorption of acetylene (C₂H₂) from the terrace has a large barrier of 2.57 eV, whereas acetylene (C₂H₂) dehydrogenation to ethynyl (CH-C) has a barrier of 1.28 eV; whereas cracking of acetylene (C₂H₂) to CH is easier (0.99 eV). To illustrate the hydrogenolysis process after C—C cracking in C₂H₂* or CH-C* we added the energy profile of CH_x (x=1 to 3) hydrogenation to the PED in Fig. 3(a). Hydrogenation of CH* to CH₂*, CH₂* to CH₃*, and CH₃* to CH_{4(g)} have activation energy barriers of 0.89, 0.65, and 0.84 eV, respectively.

Dehydrogenation of vinyl (CH₂-CH) to acetylene (C₂H₂) has a barrier of 0.89 eV, which is comparable to the barrier of vinyl hydrogenation to ethylidene (CH₃-CH) (0.89 eV). This comparison suggests that if there is H available (e.g. co-feeding H₂ in experiments), ethylidene (CH₃-CH) could be formed via vinyl (CH₂-CH) hydrogenation. We note that ethyl (C₂H₅) dehydrogenation to ethylidene (CH₃-CH) is less favorable than ethyl dehydrogenation to ethylene (C₂H₄) and thus ethylidene formation via vinyl (CH₂-CH) hydrogenation might be the dominant pathway, if there is hydrogen available. The dehydrogenation of ethylidene (CH₃-CH) to ethidyne (CH₃-C) is a facile process—only a 0.23 eV energy barrier is required. We also note that ethidyne (CH₃-C) is stable on Pt(433) terrace. Further

dehydrogenation of ethylidyne ($\text{CH}_3\text{-C}$) or cracking it into CH_3 and C has a high energy barrier (1.27 and 1.91 eV, respectively). These results suggest that, once formed, $\text{CH}_3\text{-C}$ might be a stable spectator species in this chemistry.

The PED plotted in Fig. 3(a) is based on the total energies calculated by DFT at 0 K. To probe the temperature effect and compare the DFT results with reaction kinetic experiments which were conducted at 873 K, we calculated the Gibbs free energies of all intermediates and transition states at 873 K. The diagram based on Gibbs free energies at 873 K is plotted in Fig. 3(b). The entropies of physisorbed ethane (C_2H_6^*) and methane (CH_4^*) on the Pt terrace are estimated by $S_{\text{ad}}(\text{T}) = 0.56 * S_{\text{gas}}(\text{T}) - 2R$ using Campbell's fitting parameters of ethane on Pt(111),⁴⁹ as the entropy of physisorbed ethane (C_2H_6^*) calculated within DFT is believed to be significantly underestimated. By comparing the energetics in Figs. 3(a) and (b), we find that the variation in activation energy barriers is within about 0.2 eV. However, temperature changes the energetics of gas phase ethylene (C_2H_4) and acetylene (C_2H_2), due to the entropy gain upon desorption. This change leads to a Gibbs free energy of gas phase ethylene (C_2H_4) which is 0.62 eV lower than that of adsorbed ethylene, indicating that at 873 K, ethylene readily desorbs from the surface as opposed to its further dehydrogenation to vinyl (C_2H_3^*). We conclude that ethylene (C_2H_4) is the main gas-phase product for ethane (C_2H_6) dehydrogenation on the Pt(433) terrace.

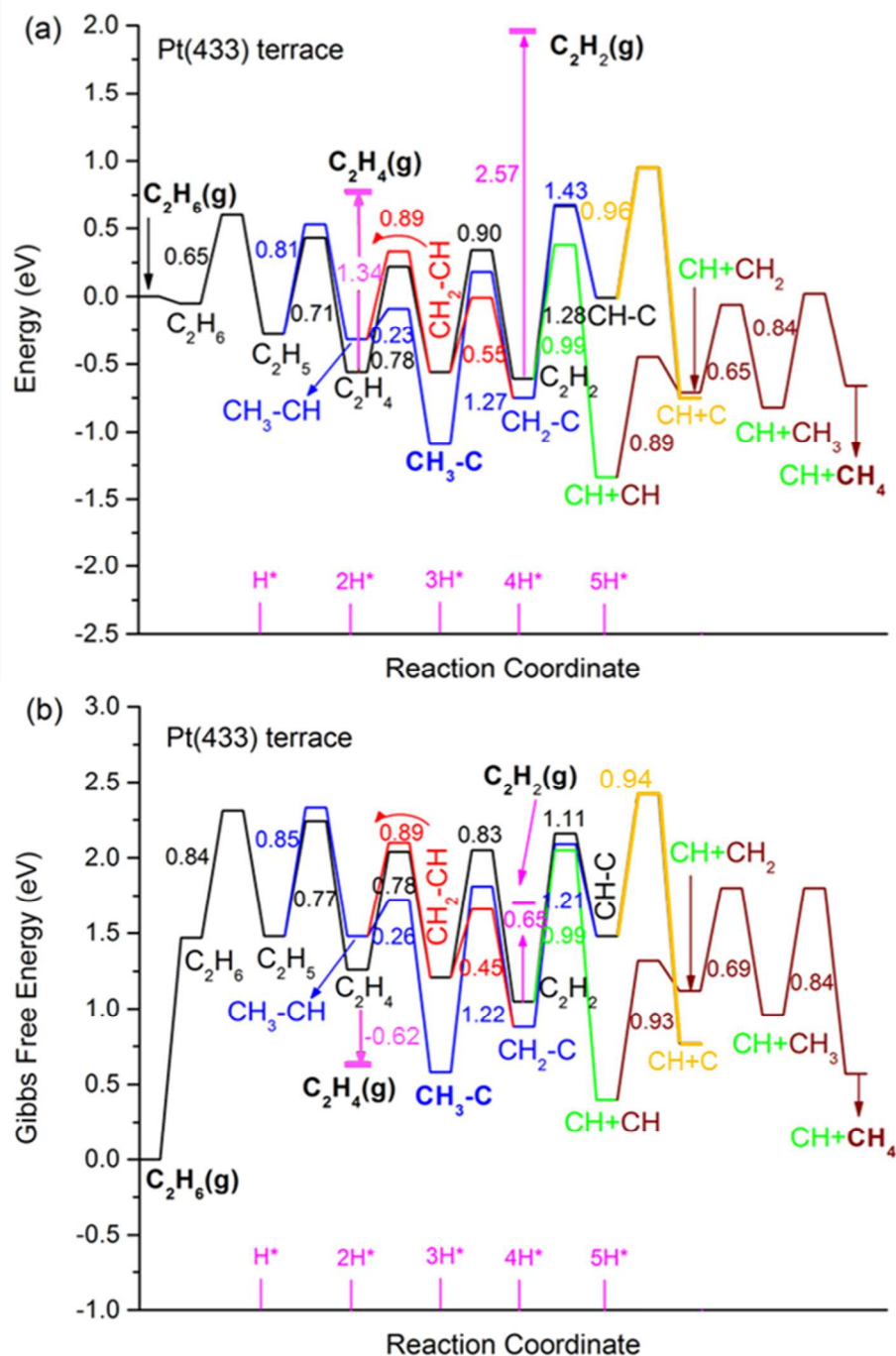


Figure 3. Ethane dehydrogenation on the terrace of Pt(433): (a) Potential energy diagram based on total energies at 0 K, and (b) Gibbs free energies calculated at 873 K. Total energies (Gibbs free energies) of clean Pt(433) surface and gas phase ethane (C_2H_6) are used as references in (a) and (b), respectively. nH^* in the bottom x axis indicates the number of co-adsorbed H atoms on the surface (at infinite separation between each other). For hydrogenation steps from CH to CH_4 , the nH^* notation was dropped for simplicity. Black line denotes $C_2H_6 \rightarrow C_2H_6^* \rightarrow C_2H_5^*+H^* \rightarrow C_2H_4^*+H^* \rightarrow CH_2-CH^*+H^* \rightarrow C_2H_2^*+H^* \rightarrow CH-C^*+H^*$, blue line denotes $C_2H_5^*+H^* \rightarrow CH_3-CH^*+H^* \rightarrow CH_3-C^*+H^* \rightarrow CH_2-C^*+H^* \rightarrow CH-C^*+H^*$, red line denotes $CH_3-CH^*+H^* \rightarrow CH_2-CH^*+H^* \rightarrow CH_2-C^*+H^*$, green line denotes $C_2H_2^* \rightarrow CH^*+CH^*$, orange line denotes $CH-C \rightarrow CH^*+C^*$, vertical pink lines denote $C_2H_4^* \rightarrow C_2H_4(g)$ and $C_2H_2^* \rightarrow C_2H_2(g)$ and the brown line denotes $CH_4 \rightarrow CH_3^*+H^* \rightarrow CH_2^*+H^* \rightarrow CH^*+H^*$ (from right to left).

3.3. Ethane dehydrogenation at the Pt(433) step edge

As discussed in section 3.1, the under-coordinated sites at the step edge of Pt(433) bind C_2H_x more strongly than the sites on the terrace and are expected to be more reactive for ethane (C_2H_6) dehydrogenation, thereby facilitating deep dehydrogenation to form undesirable coke precursors. To address this question, we studied all 29 elementary steps at the step edge, as we presented above for the terrace. In the following, we discuss in detail only the key elementary steps at the step edge.

Elementary steps for ethane dehydrogenation at the step edge

(1) *Ethane (C_2H_6) to ethyl (C_2H_5)*. Physisorbed ethane (C_2H_6) moves closer to the step and binds with ethyl (C_2H_5) bound atop Pt and H in the adjacent bridge site at the step. At the transition state, the active H is at an off-top Pt site with a H—Pt distance of 1.64 Å; the C—H bond length is 1.48 Å; and the C—Pt distance is 2.27 Å. This step is exothermic by -0.35 eV and has an activation energy barrier of 0.33 eV. Compared with the same step on terrace ($\Delta E = -0.16$ eV, $E_a = 0.65$ eV), this step is significantly facilitated at the step edge.

(2) *Ethyl (C_2H_5) to ethylene (C_2H_4)*. Dehydrogenation of ethyl (C_2H_5) to ethylene (C_2H_4) at the step is exothermic by -0.64 eV, as compared to -0.22 eV on the terrace. The activation energy barrier is 0.27 eV at the step edge, which is 0.44 eV smaller than on terrace. At the transition state, H is at an off-top Pt site; the H—Pt, H—C, C—Pt distance is 1.62, 1.48, and 2.33 Å, respectively.

(3) *Ethylene (C_2H_4) to vinyl (CH_2-CH)*. This elementary step is exothermic by -0.18 eV, as compared to 0.09 eV endothermic on the terrace. The activation energy barrier is 0.42 eV, which is 0.36 eV less than the respective barrier on the terrace. At the transition state, the active H is atop of Pt and one C moves to the bridge site at the step edge. The H—Pt and H—C distances are 1.64 and 1.51 Å, respectively. The final state of this elementary step has H at the step-bridge site and vinyl (CH_2-CH) at top-bridge on the step edge.

(4) *Vinyl (CH_2-CH) to acetylene (C_2H_2)*. Dehydrogenation of vinyl (CH_2-CH) to acetylene (C_2H_2) is nearly thermoneutral at the step edge. The total activation energy barrier is 1.29 eV, as opposed to a 0.90 eV on the terrace. This dehydrogenation involves a transformation of vinyl (CH_2-CH) from a top (at step)-bridge site (at step) to a less stable (by 0.24 eV) top (at terrace)-bridge (at step edge) configuration, with an activation energy barrier of 0.71 eV. H abstraction takes place from this less stable intermediate state and ends up with acetylene at the bridge-bridge site and the H at the step-bridge site, with an activation energy barrier of 1.05 eV. Therefore, the overall activation energy barrier of this dehydrogenation process is 1.29 eV.

(5) *Ethyl (C_2H_5) to ethylidene (CH_3-CH)*. This step is exothermic (-0.62 eV) at the step edge versus nearly thermoneutral on the terrace (0.04 eV). The activation energy barrier at the step edge is 0.08 eV, which is much smaller than that on the terrace (0.81 eV). This result suggests that at the step edge, in

contrast to the case on the terrace, dehydrogenation of ethyl (C_2H_5) to ethylidene (CH_3-CH) is faster than dehydrogenation from ethyl to ethylidene's isomer ethylene (C_2H_4) (0.27 eV).

(6) *Vinyl (CH_2-CH) to ethylidene (CH_3-CH)*. Vinyl (CH_2-CH) hydrogenation to ethylidene (CH_3-CH) at the step edge has an activation energy barrier of 0.97 eV and a reaction energy of 0.30 eV. The energy barrier is 0.17 eV higher than the barrier of the same process on the terrace.

(7) *Ethylidene (CH_3-CH) to ethylidyne (CH_3-C)*. Dehydrogenation of ethylidene (CH_3-CH) to ethylidyne (CH_3-C) at the step is an exothermic process (-0.40 eV), with an activation energy barrier of 0.73 eV, which is 0.5 eV higher than the energy barrier for the same step on the terrace. This behavior can be understood by considering the binding energy change at the step edge compared with that on the terrace: the binding energy of ethylidene (CH_3-CH) at the step is increased by 0.55 eV, whereas the binding energy of ethylidyne (CH_3-C) at the step is similar to that on the terrace (see Table 1).

(8) *Ethylidyne (CH_3-C) to vinylidene (CH_2-C)*. The dehydrogenation of ethylidyne (CH_3-C) to vinylidene (CH_2-C) is endothermic by 0.10 eV at the step edge and has an activation energy barrier of 0.89 eV, versus a barrier of 1.27 eV on the terrace.

(9) *Vinyl (CH_2-CH) to vinylidene (CH_2-C)*. This dehydrogenation step is endothermic by 0.08 eV with an activation energy barrier of 0.81 eV, which is higher than the respective on the terrace (0.55 eV).

(10) *Vinylidene (CH_2-C) to ethynyl ($CH-C$)*. The dehydrogenation of vinylidene (CH_2-C) to ethynyl ($CH-C$) is endothermic by 0.37 eV and has an activation energy barrier of 1.41 eV at the step edge, which is similar to what was found on the terrace (1.43 eV).

(11) *Acetylene (C_2H_2) to ethynyl ($CH-C$)*. Breaking one C—H bond in acetylene (C_2H_2) to form ethynyl ($CH-C$) is endothermic by 0.51 eV and has an activation energy barrier of 1.49 eV at the step edge, suggesting that this step is easier on the terrace (1.28 eV).

(12) *Ethynyl ($CH-C$) to CC*. The abstraction of the last H is endothermic by 0.67 eV, with an activation energy barrier of 1.40 eV. The activation energy barrier is 0.18 eV lower than the barrier of the same elementary step on the terrace.

The three C_2 isomerization processes, i.e., elementary steps: (13) ethylene (C_2H_4) to ethylidene (CH_3-CH), (14) vinyl (CH_2-CH) to ethylidyne (CH_3-C), and (15) vinylidene (CH_2-C) to acetylene (C_2H_2) at the step edge were also studied and the calculated activation energy barriers are 2.24, 2.02, and 2.36 eV, respectively. On the terrace, the activation energy barriers of steps (13), (14) and (15) were 2.12, 2.00 and 2.50 eV, respectively.

All calculated activation energy barriers and reaction energies for these above-mentioned 15 elementary steps at the step edge of Pt(433) are provided in Table 2, for direct comparison with their energetics on the terrace.

Elementary steps for C—C bond breaking at the step edge

The results for all possible C—C bond breaking steps in C_2H_x species at the step edge are summarized in the appropriately designated columns of Table 3 (steps 16-25). Similar to what we found on the terrace, at the step edge, C—C bond breaking steps before reaching the adsorbed acetylene ($C_2H_2^*$) state, are generally more difficult than dehydrogenation steps. For example, C-C bond breaking in ethane (C_2H_6), ethyl (C_2H_5), and ethylene (C_2H_4) are taking place easier at the step edge than on the terrace, with activation energy of barriers of 1.99, 1.58, and 1.53 eV, respectively. For comparison, ethane (C_2H_6) dehydrogenation to ethyl (C_2H_5), ethyl hydrogenation to ethylene (C_2H_4) (or to ethylidene (CH_3-CH)), and ethylene dehydrogenation to vinyl (CH_2-CH) have activation energy barriers of 0.33, 0.27 (or 0.08), and 0.42 eV, respectively. Further, and similar to what we found on the terrace, C—C bond breaking in adsorbed acetylene ($C_2H_2^*$) and adsorbed ethynyl ($CH-C^*$) at the step edge has barriers lower than dehydrogenation of these species (see step 11 and 12 in Table 2): C—C bond breaking in $C_2H_2^*$ and $CH-C^*$ at the step edge has a barrier of 1.35 and 1.00 eV, respectively; whereas C—H bond breaking in $C_2H_2^*$ and $CH-C^*$ at the step edge has a barrier of 1.49 and 1.40 eV, respectively.

Dehydrogenation of CH_x ($x=1-4$) species at the step edge

The reaction energies and activation energy barriers calculated for dehydrogenation of CH_x species at the step edge are tabulated in Table 3 (steps 26, 27, 28 and 29). The reverse reaction steps of 26, 27, and 28 lead to methane (CH_4) formation. The activation energy barriers for the first, second, third, and fourth dehydrogenation steps of methane (CH_4) at the step edge (steps 26-29) are 0.28, 0.13, 0.68 and 1.08 eV respectively.

Potential energy diagram for ethane dehydrogenation at the Pt(433) step edge

Plotted in Fig. 4(a) is the potential energy diagram of ethane dehydrogenation at the step edge of Pt(433) based on the total energies calculated at 0 K. Analysis of the path $C_2H_6^* \rightarrow C_2H_5^* + H^* \rightarrow C_2H_4^* + 2H^* \rightarrow CH_2-CH^* + 3H^* \rightarrow C_2H_2^* + 4H^*$ (black line) shows that at the step edge, ethane (C_2H_6) is dehydrogenated to ethylene (C_2H_4), which is further dehydrogenated to vinyl (CH_2-CH) (barrier of 0.42 eV) rather than desorbing to the gas phase due to a higher desorption barrier (1.73 eV). Further, vinyl (CH_2-CH) dehydrogenation to acetylene (C_2H_2) (barrier of 1.30 eV) is energetically less favorable than its hydrogenation to ethylidene (CH_3-CH) (barrier of 1.06 eV). At the step edge, acetylene (C_2H_2) binds strongly (binding energy of 2.93 eV), suggesting that C-C bond breaking in C_2H_2 is easier than desorption. To illustrate the hydrogenolysis process after C—C cracking in $C_2H_2^*$ or $CH-C^*$ we added the energy profile of CH_x ($x=1$ to 3) hydrogenation to the PED in Fig. 3(b). Hydrogenation of CH^* to

CH_2^* , CH_2^* to CH_3^* , and CH_3^* to $\text{CH}_{4(\text{g})}$ have activation energy barriers of 0.96, 0.64, and 0.86 eV, respectively.

To probe the temperature and entropy effects, we then generated the Gibbs free energy diagram at 873 K (see Fig. 4(b)). Because C_2H_6^* and CH_4^* adsorbed at the step edge can be viewed as 1D gases (i.e., they lose of all translational entropy except the one along the direction of the step edge), their entropy at the Pt step edge was estimated by the respective value on the terrace minus 1D translational entropy, i.e., $S_{\text{ad}}(\text{step}, T) = 0.56 * S_{\text{gas}}(T) - 2R - S_{1\text{D-trans}}(T)$.

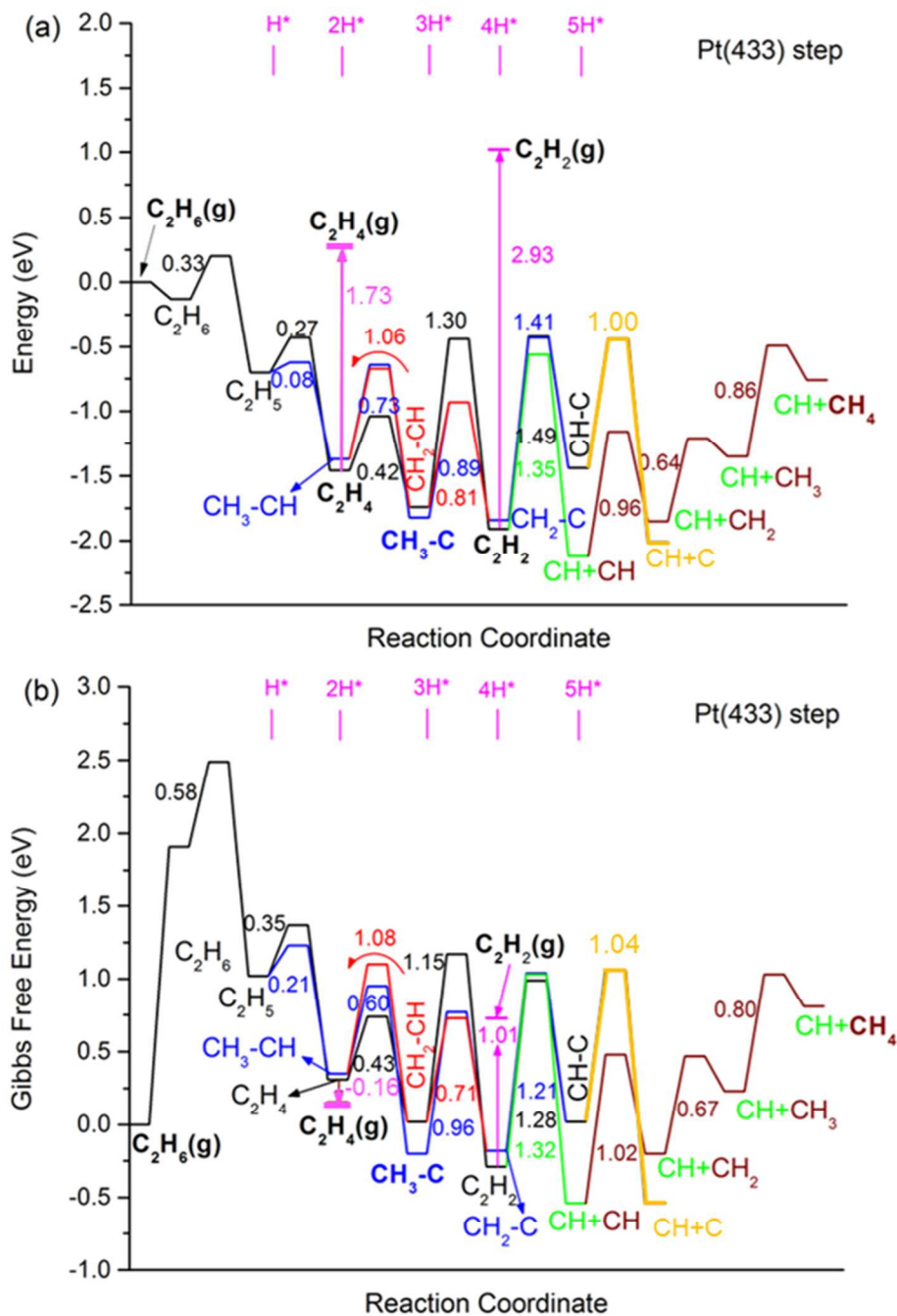


Figure 4. Ethane dehydrogenation at the step edge of Pt(433): (a) Potential energy diagram based on total energies at 0 K and (b) Gibbs free energies calculated at 873 K. Total energies (Gibbs free energies) of clean Pt(433) surface and gas phase ethane (C_2H_6) are used as references in (a) and (b), respectively. nH^* in the top x axis indicates the number of co-adsorbed H on the surface (at infinite separation from each other). For hydrogenation steps from CH to CH_4 , the nH^* notation was dropped for simplicity. For description of the color scheme refer to Figure 3.

A comparison of the energy diagrams in Figs. 4(a) and (b) shows that the temperature effect (at 873 K) on the barrier of surface reaction steps is within 0.2 eV. Similar to what we found on the terrace, the temperature changes the energetics of gas phase species ethane, ethylene and acetylene (C_2H_6 , C_2H_4 and C_2H_2) due to entropy changes. In particular, the Gibbs free energy of gas phase ethylene (C_2H_4) is 0.16 eV below that of $C_2H_4^*$. At 873 K, dehydrogenation of $C_2H_4^*$ has a barrier of 0.43 eV at the step edge. This result suggests that at 873 K, desorption of ethylene (C_2H_4) from the step edge is preferred to its dehydrogenation by 0.59 eV. For comparison, on the terrace, the transition state Gibbs free energy for dehydrogenation of adsorbed ethylene ($C_2H_4^*$) is 1.40 eV higher in energy than gas phase ethylene (C_2H_4), suggesting that selectivity towards desorption of ethylene is higher at the terrace than at the step edge.

Further, ethyl (C_2H_5) dehydrogenation to ethylidene (CH_3-CH) is easier than ethylene (C_2H_4) formation at the step edge. Ethylidene (CH_3-CH) can be further dehydrogenated to ethylidyne (CH_3-C) with a barrier of 0.60 eV at 873 K. Both ethylidyne (CH_3-C^*) and vinylidene (CH_2-C^*) are stable and thus will likely accumulate at the step edge. These intermediates may serve as seeds for subsequent formation of coke or other carbon-containing species such as graphene²¹ and eventually lead to Pt catalyst deactivation.

One possible strategy to mitigate coke formation and prevent catalyst deactivation from coke formation, would therefore be to block the highly reactive under-coordinated step edge sites. This strategy was successfully employed to stabilize Pd catalysts for oxidative dehydrogenation of ethane to ethylene³² and Cu catalysts for liquid-phase reactions³⁵ by overcoating the surface with alumina moieties using atomic layer deposition. The enhanced stability was assigned to the selective decoration of under-coordinated copper atoms on the nanoparticles' surface. Inspired by that work, in the next section, we discuss ethane dehydrogenation on alumina-decorated Pt(433).

3.4. Ethane dehydrogenation on AlO_x -decorated Pt(433)

To investigate the effect of AlO_x decoration of Pt catalysts used in ethane dehydrogenation, we considered six different AlO_x decorated Pt(433) models, as shown in Fig. 5. We calculated the surface energy according to^[50]

$$\gamma(T, P) = \frac{1}{A} [G_{\text{Pt}}^{\text{AlO}_x}(T, p) - G_{\text{Pt}}(T, P) - N_{\text{Al}}\mu_{\text{Al}} - N_{\text{O}}\mu_{\text{O}}],$$

where $G_{\text{Pt}}^{\text{AlO}_x}(T, p)$ and $G_{\text{Pt}}(T, P)$ are Gibbs free energies of AlO_x decorated and pristine Pt(433) surfaces, respectively; A is the surface area of the respective model; N_{Al} (N_{O}) and μ_{Al} (μ_{O}) are the number and chemical potential of Al (O) atoms decorating the Pt(433) surface, respectively. Assuming that there is sufficient bulk Al_2O_3 material to act as a thermodynamic reservoir, the chemical potential of O and Al are related to each other by the Gibbs free energy of the bulk oxide

$$2\mu_{\text{Al}}(T, P) + 3\mu_{\text{O}}(T, P) = g_{\text{Al}_2\text{O}_3}^{\text{bulk}}(T, P).$$

In this framework, vibrational energy and entropy contributions are neglected and the Gibbs free energies are approximated by the total energies calculated by DFT. This approximation has been shown to be accurate enough for oxides in previous studies.^[50–52] The relation of O chemical potential and the pressure of O_2 at a given temperature T is given by:

$$\mu_{\text{O}}(T, P) = \mu_{\text{O}}(T, P^0) + \frac{1}{2} k_b T \ln \left(\frac{P}{P^0} \right),$$

where $\mu_{\text{O}}(T, P^0)$ can be calculated using data from thermochemical tables at $P^0 = 1 \text{ atm}$.^[1]

Plotted in Fig. 6 are the surface energies of the models considered in this study as a function of the oxygen chemical potential ($\Delta\mu_{\text{O}} \equiv \mu_{\text{O}} - \frac{1}{2} E_0(\text{O}_2)$, where $E_0(\text{O}_2)$ is the total energy of gas phase O_2).

The O_2 pressure at $T=500 \text{ K}$ is calculated using data from thermochemical tables and shown in the top x axis. Figure 6 suggests that model (e) with Al_6O_{11} decoration of the Pt(433) step edge is the most stable model over a wide range of O chemical potential. We thus choose Al_6O_{11} -decorated Pt(433) as our model system for the alumina-overcoated Pt catalysts used in our subsequent experiments. We note that other models with different stoichiometry, size, or geometry could be also stable. Since the real atomic structure of the alumina decoration in the catalysts is unknown, the Al_6O_{11} -decorated Pt(433) system serves as a reasonable starting model for evaluating the effect of alumina overcoating of Pt catalysts on ethane dehydrogenation reactivity.

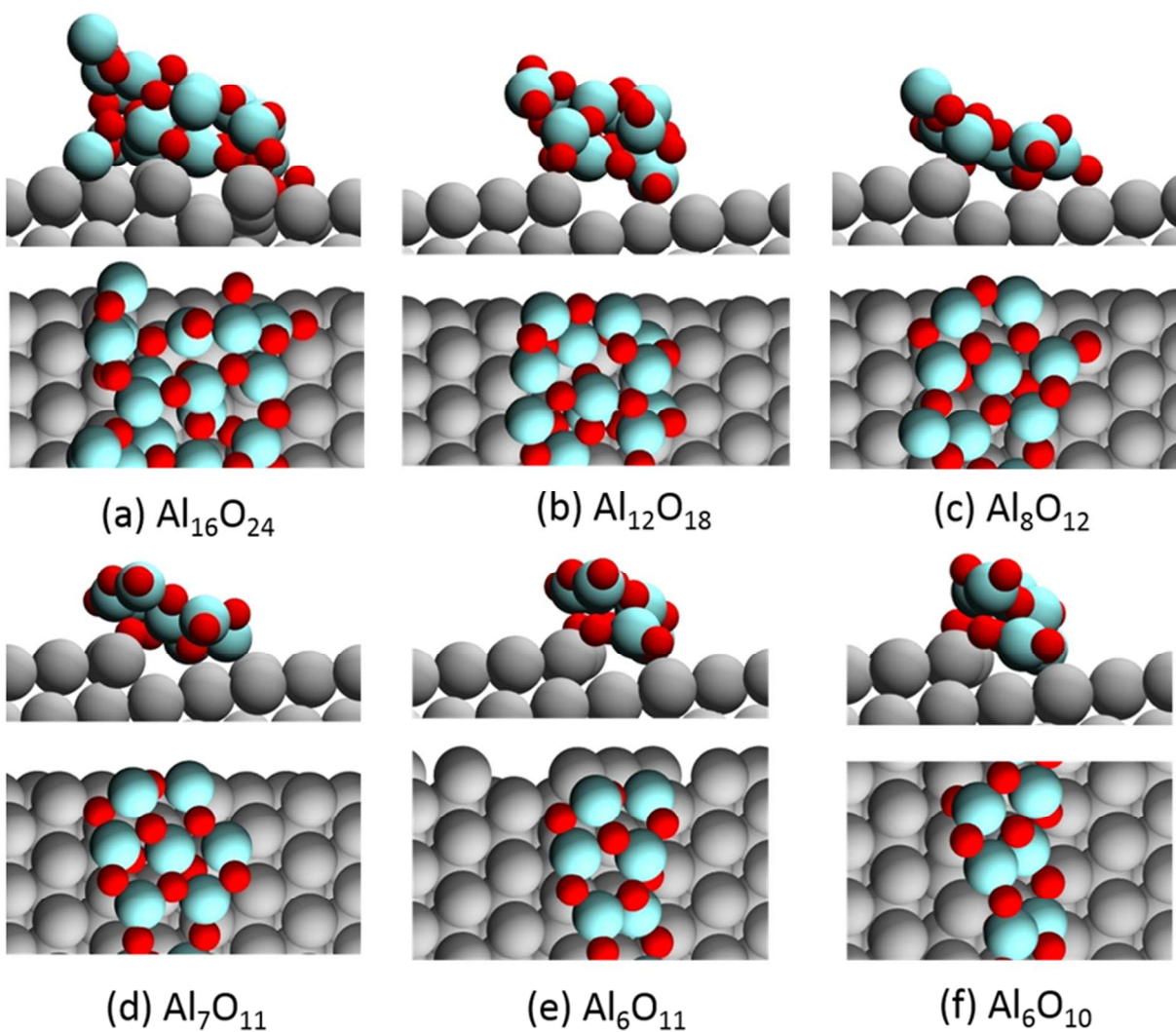


Figure 5. Cross-section and top views of different models considered for AlO_x -decorated Pt(433). Gray, cyan and red spheres denote Pt, Al, and O, respectively.

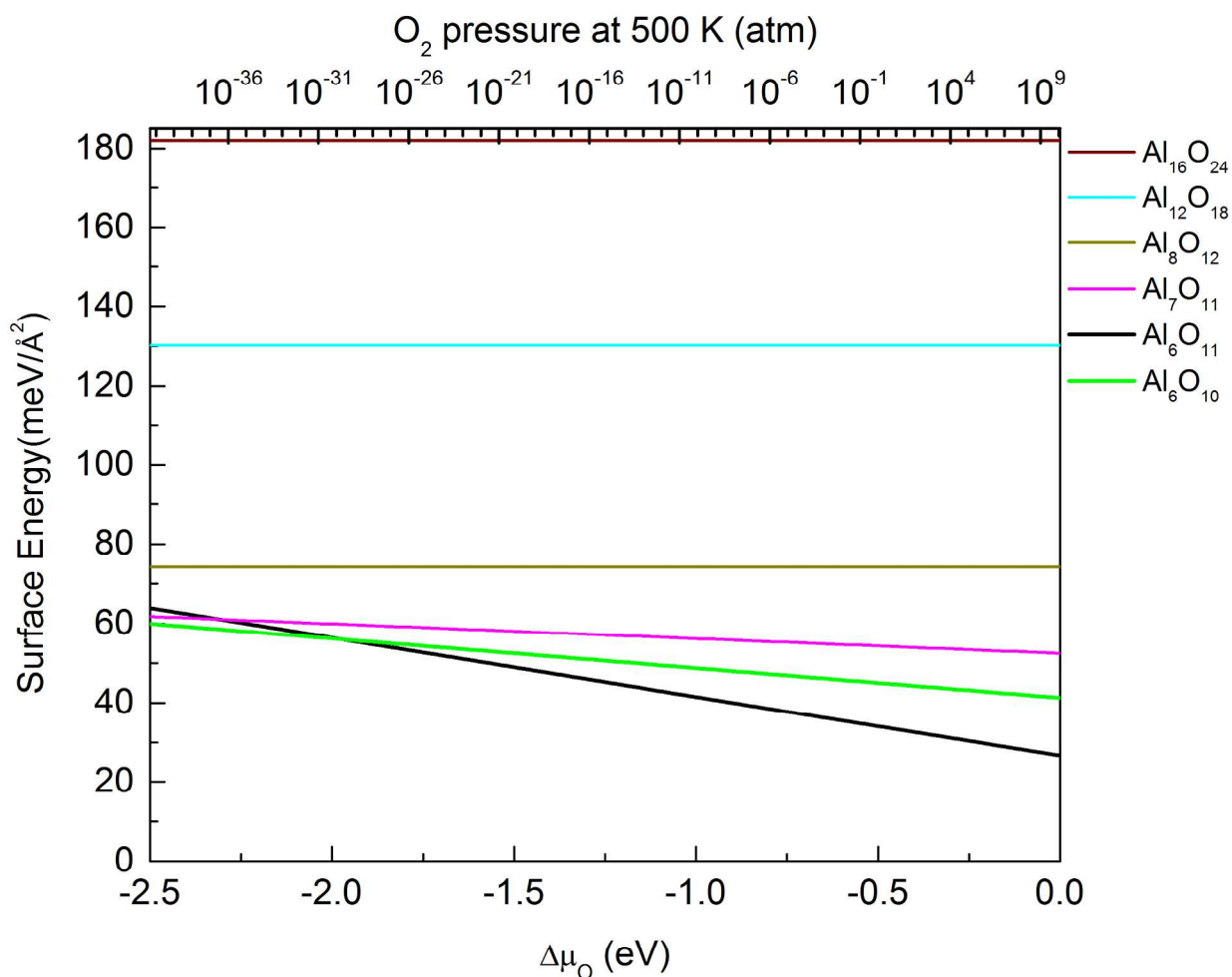


Figure 6. Calculated surface energy γ as a function of oxygen chemical potential for six different AlO_x -decorated Pt(433) models shown in Figure 5. The total energy of gas phase O_2 , $\frac{1}{2}E_0(\text{O}_2)$, is used as zero reference. O_2 pressure at $T=500$ K is calculated and shown in top x axis.

We then studied the adsorption of C_2H_x and CH_x species on the Al_6O_{11} -decorated Pt(433). Because the step was coated by Al_6O_{11} , the reactivity of the model surface will be dominated by that of the uncovered terrace of Pt(433). The calculated binding preference and binding energy of different species are summarized in the Al_6O_{11} decorated Pt(433) columns of Table 1. Our results suggest that the Al_6O_{11} decoration has minimal effect on the binding preferences and binding energies of species on the terrace. Compared with the data on the terrace of the pristine Pt(433) surface (see Table 1), the binding energy change on the Al_6O_{11} -decorated Pt(433) is small.

With similar binding preference and small change in binding energy of C_2H_x and CH_x species on the terrace of the Al_6O_{11} decorated Pt(433) surface, we expect the reaction energies and energy barriers of all 29 elementary steps for ethane dehydrogenation and C-C bond breaking would be similar to those on the terrace of the pristine Pt(433) surface. To examine this hypothesis, we studied all 29 elementary steps on the terrace of the Al_6O_{11} decorated Pt(433) surface. The results are summarized in the Al_6O_{11}

decorated Pt(433) columns of Tables 2 and 3. Our calculations showed that the changes in reaction energies and binding energies between the two model surfaces are small and typically within 0.2 eV. This behavior is because the Al_6O_{11} decorated surface has four-atom wide terraces unperturbed by the presence of Al_6O_{11} and the interaction between Al_6O_{11} and the adsorbed species is minimal.

Figure 7(a) provides the PED for ethane (C_2H_6) dehydrogenation on the Al_6O_{11} decorated surface at 0 K. This PED is similar to that derived for the terrace of the pristine Pt(433) surface, Fig. 3(a). Accordingly, the respective Gibbs free energy diagram for the Al_6O_{11} -decorated Pt(433) surface calculated at 873 K (Fig. 7(b)) is also similar to Fig.3(b). These results suggest that the Al_6O_{11} decoration of the step edge does not change the thermodynamics and kinetics of ethane (C_2H_6) dehydrogenation and cracking on the Pt terrace. However, the Al_6O_{11} decoration of the step edge, blocks the facile dehydrogenation channel which was found at the pristine step edge, and was responsible for the formation of coke precursors. The Al_6O_{11} decoration forces reactions to take place on the terrace, where as shown earlier above, coke formation becomes much more difficult than on the step edge, leading to ethylene (C_2H_4) as the main gas phase product.

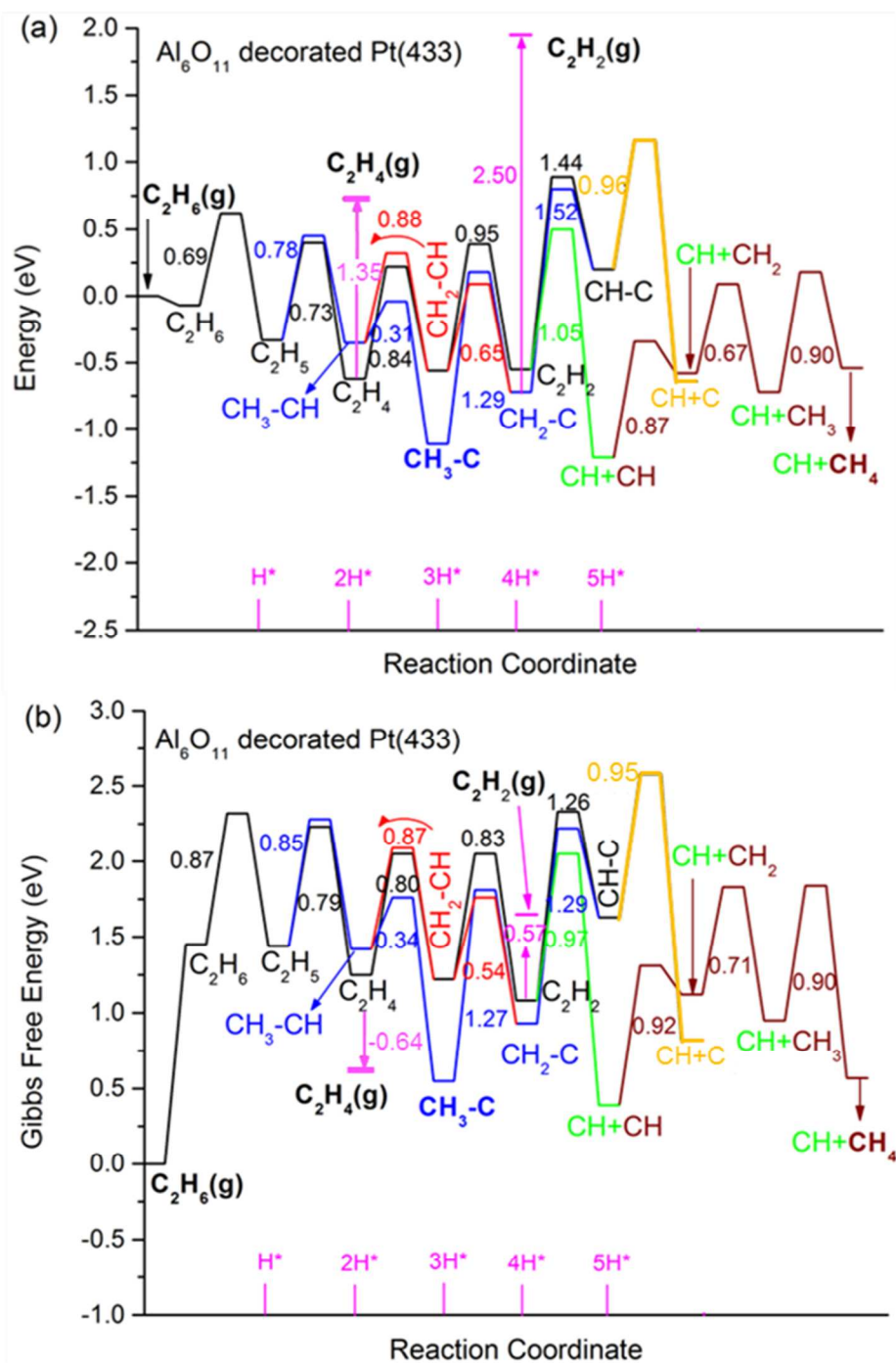


Figure 7. Ethane dehydrogenation on Al_6O_{11} -decorated Pt(433): (a) Potential energy diagram based on total energies at 0 K, and (b) Gibbs free energies calculated at 873 K. Total energies (Gibbs free energies) of clean Al_6O_{11} -decorated Pt(433) surface and gas phase ethane (C_2H_6) are used as references in (a) and (b), respectively. $n\text{H}^*$ in the top x axis indicates the number of co-adsorbed H on the surface (at infinite separation from each other). For hydrogenation steps from CH to CH_4 , the $n\text{H}^*$ notation was dropped for simplicity. For description of the color scheme refer to Figure 3.

3.5. Reaction kinetics studies

To study the hypothesis formulated on the basis of our DFT results for the effect of alumina overcoats on the reactivity of supported Pt catalysts for ethane (C_2H_6) dehydrogenation, we performed reaction kinetic studies of ethane dehydrogenation on supported Pt catalysts, both pristine and ALD alumina overcoated.

Catalyst regeneration: In general, there are two main paths to catalyst deactivation: (i) sintering, leading to formation of large metal particles, and (ii) coking, which is characterized by deposition of carbonaceous species. Sintering is irreversible, but coking can be reversed with calcination. The interaction of hydrocarbons with metal surfaces usually results in the formation of a carbonaceous layer.^[53,54] ALD of alumina overcoat on supported metal catalysts has been shown to be effective in preventing catalyst deactivation due to coking and sintering. For instance, 45 cycles of ALD alumina overcoating on Pd/ Al_2O_3 was shown to reduce coke formation by 94% and suppress sintering during catalytic oxidative dehydrogenation of ethane.^[32] Also, ALD alumina overcoat enhanced methanol decomposition activity of Pd catalysts by preferentially nucleating at corners, steps and edges of the Pd nanoparticles and preventing loss of active surface area during the reaction.^[33] Similarly, alumina overcoating has been shown to stabilize Cu catalysts for liquid phase catalytic reactions; the hypothesis is that this improvement is caused by selectively armoring the under-coordinated Cu sites on the nanoparticle surface with alumina species.^[35]

To test the regenerability of our catalyst, we performed a series of experiments on the same catalyst sample, consisting of reduction-reaction-regeneration steps that were repeated consecutively. Figure 8 shows the measured ethylene TOF as a function of time on stream over a 10cALD/Pt/ γ - Al_2O_3 catalyst in a continuous flow reactor following first, second and third regenerations respectively.

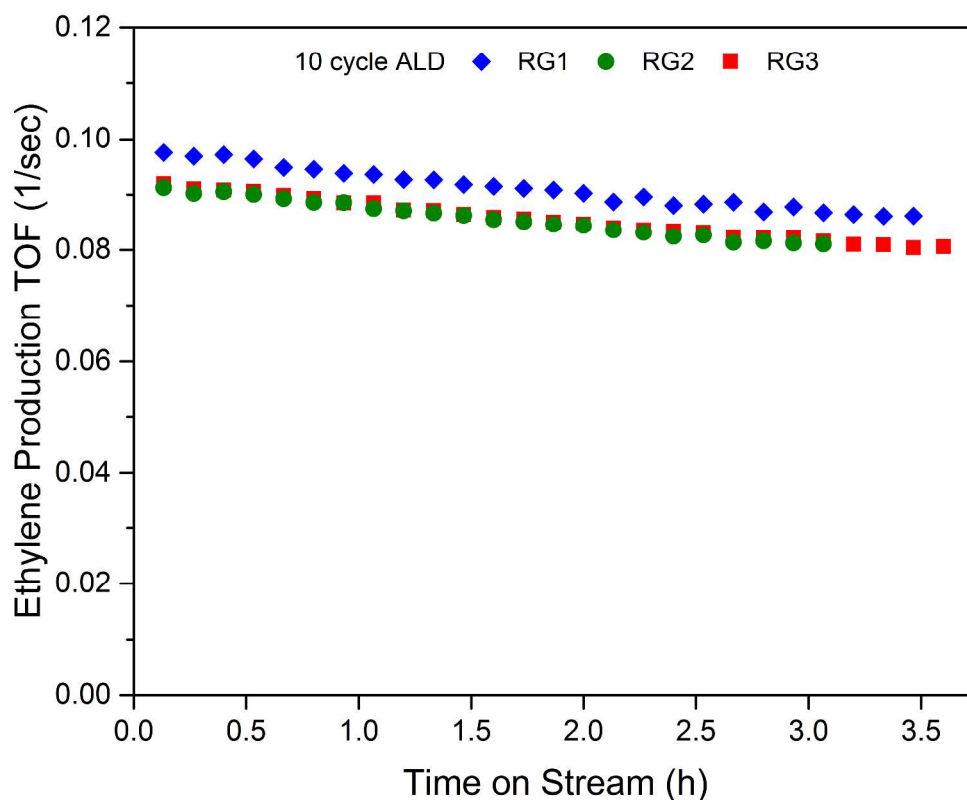


Figure 8. Ethylene production TOF as a function of time on stream on a 10cALD/ Pt/ γ -Al₂O₃ catalyst (after: one regeneration [RG1] \blacklozenge ; two regenerations [RG2] \bullet ; three regenerations [RG3] \blacksquare). Reaction conditions: 873 K, 12.5 Torr ethane, 0 Torr hydrogen, and balance helium for a total pressure of 1 atm.

The results shown in Figure 8 suggest that the catalyst activity is largely reversed upon calcination, indicating that the deactivation is primarily due to coking.

This regeneration-reduction-reaction cycle was carried out for the non-overcoated Pt/ γ -Al₂O₃ catalyst and a similar pattern was observed. Thus, both catalysts are stable and reusable over repeated calcination-reduction-reaction cycles. The TOF for ethylene production as a function of time for fresh and RG3 (after three regenerations) non-overcoated Pt/ γ -Al₂O₃ catalysts is shown in Figure S1 in Supplementary Information. Also, prior to the first regeneration step, CO chemisorption was performed on spent non-overcoated Pt/ γ -Al₂O₃ sample. It was observed that the extent of CO adsorption on the catalyst at the end of reaction decreased from 28 $\mu\text{mol/g}$ to 17 $\mu\text{mol/g}$ cat due to coke deposition.

Effect of alumina overcoating. Figure 9 shows ethylene TOF versus time on stream for both catalysts after three regenerations. After 3 h on stream and in the absence of hydrogen, the 10cALD/Pt/ γ -Al₂O₃ catalyst exhibited ~4 times higher ethylene TOF compared to the non-overcoated Pt/ γ -Al₂O₃ catalyst.

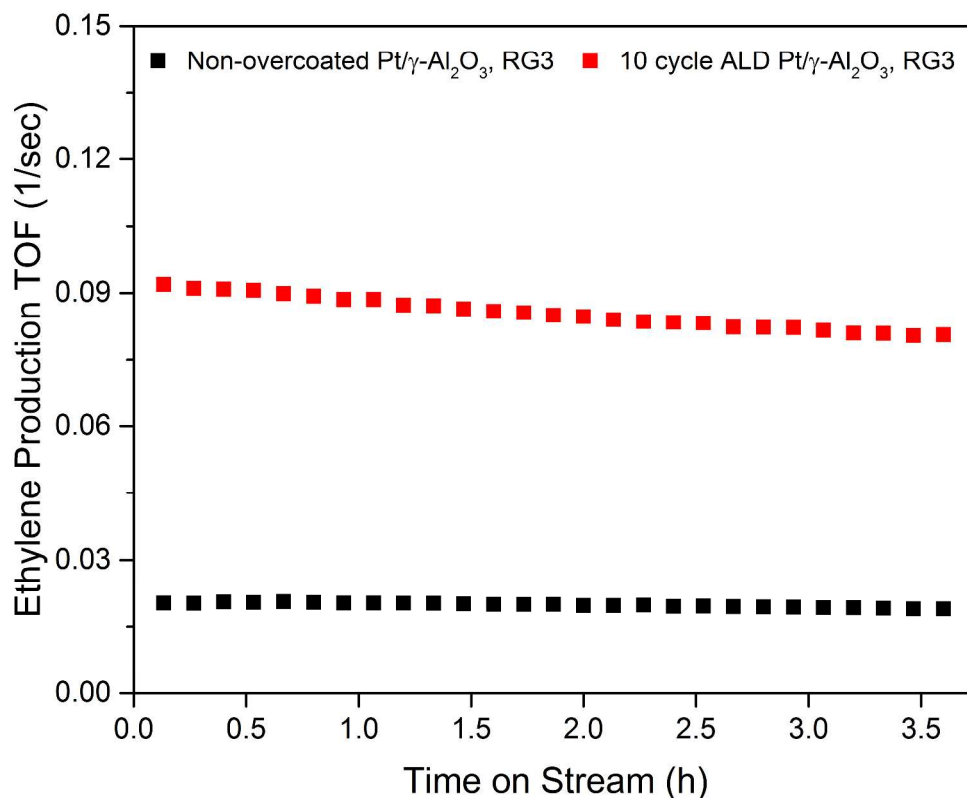


Figure 9. Ethylene production TOF versus time on stream on: non-overcoated Pt/ γ -Al₂O₃ (■) and 10cALD/Pt/ γ -Al₂O₃ (■) catalysts after three catalyst regenerations. Reaction conditions: 873 K, 12.5 Torr ethane, 0 Torr hydrogen, and balance He for a total pressure of 1 atm.

Coke quantification. Alumina-supported Pt is a well-known industrial catalyst for paraffin dehydrogenation. In addition to the metal sites, the acidic sites on the high surface area alumina accelerate hydrogenolysis, isomerization, and enhance coke formation.^[55] There has been extensive research on the use of modifiers like Sn and Re on oxide-supported Pt catalysts as they help with to suppress coke deposition.^[25,56] This improvement has been attributed to both geometric and electronic effects. The addition of modifiers prevents the formation of certain surface Pt atom ensembles, which translates into weaker binding of coke precursor species to the active site.^[57,58] Calculations in the present study suggest that Pt edges adsorb coke precursors strongly, but when these edges are decorated with AlO_x, then coke precursors can no longer adsorb to the edges, but only to terraces, where desorption is enhanced compared to further dehydrogenation toward coke formation.

To probe this theoretical prediction, we set to experimentally quantify catalyst deactivation due to coke formation by utilizing thermogravimetric analysis (TGA). The experiments aimed to collect spent catalysts for TGA were performed as described in the methods section. After 2 h in reaction with the non-overcoated Pt/ γ -Al₂O₃ catalyst, 0.98 mg of coke was formed on 24.55 mg of catalyst sample, corresponding to a loss of 4 wt%, whereas under the same conditions the 10cALD/Pt/ γ -Al₂O₃ catalyst yielded a 1.05 wt% loss. The overcoated catalyst produces less coke per mass of catalyst (see Table 4) and maintains higher activity per site, when compared to the non-overcoated catalyst (Fig. 9). It is also possible that the small amount of carbon deposited on the overcoated 10cALD/Pt/ γ -Al₂O₃ catalyst migrates to the alumina moieties located on the Pt nanoparticles, thereby allowing the Pt sites to remain active for long periods of time on stream.

Table 4: Thermogravimetric analysis for coke deposition on spent catalysts

Catalyst	CO Uptake ($\mu\text{mol sites/gcat}$)	Carbon Deposition (mmol C/gcat)
Non-overcoated 1 wt. % Pt/ γ -Al ₂ O ₃	29	3.36
10cALD/Pt/ γ -Al ₂ O ₃	3	0.87

In summary, both the non-overcoated and the overcoated catalysts prepared in this study were stable to the regeneration-reduction-reaction cycle. The coke deposited was removed by calcination and the activity was largely restored by subsequent reduction. The alumina overcoated catalyst, 10cALD/Pt/ γ -Al₂O₃, showed higher initial as well as steady state activity as compared to the non-overcoated catalyst. Thermogravimetric analysis showed a higher amount of coke formation on the non-overcoated catalyst. These experimental results verify the hypothesis formulated by our theoretical model, suggesting that alumina overcoated catalysts suppress coke formation by preferentially armoring the lower-coordinated sites of the Pt particles.

4. Conclusions

We presented a systematic mechanistic study of ethane dehydrogenation on pristine and AlO_x -decorated Pt surfaces by using DFT calculations and reaction kinetic experiments. We studied the adsorption of 14 distinct C_2H_x and CH_x species on the terrace and at the step edge of Pt(433) and determined the minimum energy paths for 29 elementary reaction steps involved in this reaction. We showed that on pristine Pt(433), compared to terrace sites, the under-coordinated step edge sites facilitate dehydrogenation leading to formation of coke precursors. We further demonstrated that by decorating the step edge with alumina species, the thermodynamics and kinetics of ethane dehydrogenation and C—C cracking on the terrace sites remains practically unchanged compared to the terrace sites of the pristine Pt surface model. Coke formation is suppressed on alumina-decorated Pt surfaces and reactivity on these catalysts is essentially confined at the alumina-free terrace sites. The results of our reaction kinetic experiments for ethane dehydrogenation on ALD alumina overcoated Pt/ γ - Al_2O_3 catalyst and Pt/ γ - Al_2O_3 showed that the 10 cycle ALD/Pt/ γ - Al_2O_3 catalyst exhibits 4 times higher ethylene turnover frequency compared to Pt/ γ - Al_2O_3 , in good agreement with our DFT results. Our results suggest that alumina-decorated supported Pt could be a promising catalyst for alkane dehydrogenation and therefore could have applications, including in endothermic fuel cooling for hypersonic flights.

Conflicts of interest

There are no conflicts to declare.

Acknowledgements

This work was supported by the Air Force Office of Scientific Research under a Basic Research Initiative grant (AFOSR FA9550-12-1-0481). The computational work was performed by using supercomputing resources at the Department of Defense (DoD) High Performance Computing Modernization Program (the US Air Force Research Laboratory DoD Supercomputing Resource Center (AFRL DSRC), the US Army Engineer Research and Development Center (ERDC), and the Navy DoD Supercomputing Resource Center (Navy DSRC)) supported by the Department of Defense. Additional CPU resources from the following institutions: EMSL, a National scientific user facility at Pacific Northwest National Laboratory (PNNL); the Center for Nanoscale Materials (CNM) at Argonne National Laboratory (ANL); and the National Energy Research Scientific Computing Center (NERSC) were used to conduct this work. EMSL is sponsored by the Department of Energy's Office of Biological and Environmental Research located at PNNL. CNM, and NERSC are supported by the U.S. Department of Energy, Office of Science, under Contracts DE-AC02-06CH11357, and DE-AC02-05CH11231, respectively. We thank Lang Xu for his valuable comments.

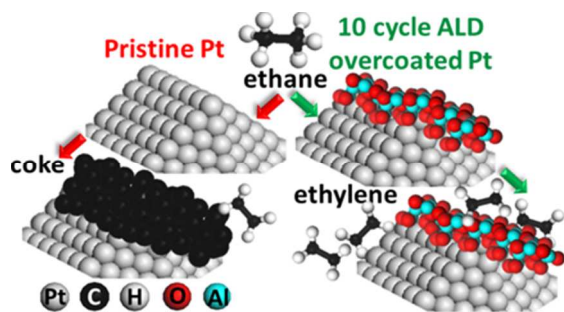
References

- [1] P. J. Linstrom, W.G. Mallard, Eds., *NIST Standard Reference Database Number 69*; National Institute of Standards and Technology: Gaithersburg MD, 20899, **2017**.
- [2] J. H. Sinfelt, W. F. Taylor, D. J. C. Yates, *J. Phys. Chem.* **1965**, *69*, 95-101.
- [3] J. H. Sinfelt, D. J. C. Yates, *J. Catal.* **1967**, *8*, 82-90.
- [4] P. Cremer, C. Stanners, J. W. Niemantsverdriet, Y. R. Shen, G.A. Somorjai, *Surf. Sci.* **1995**, *328*, 111-118.
- [5] P. S. Cremer, X. C. Su, Y. R. Shen, G. A. Somorjai, *J. Am. Chem. Soc.* **1996**, *118*, 2942-2949.
- [6] L. L. Kesmodel, L. H. Dubois, G. A. Somorjai, *J. Chem. Phys.* **1979**, *70*, 2180-2188.
- [7] R. D. Cortright, R. M. Watwe, J. A. Dumesic, *J. Mol. Catal. A-Chem.* **2000**, *163*, 91-103.
- [8] R. D. Cortright, R. M. Watwe, B. E. Spiewak, J. A. Dumesic, *Catal. Today* **1999**, *53*, 395-406.
- [9] J. J. W. Harris, V. Fiorin, C. T. Campbell, D. A. King, *J. Phys. Chem. B* **2005**, *109*, 4069-4075.
- [10] F. R. Laffir, J. J. W. Harris, V. Fiorin, D. A. King, *Chem. Phys. Lett.* **2007**, *439*, 342-347.
- [11] R. M. Watwe, H. S. Bengaard, J. R. Rostrup-Nielsen, J. A. Dumesic, J. K. Norskov, *J. Catal.* **2000**, *189*, 16-30.
- [12] R. M. Watwe, R. D. Cortright, M. Mavrikakis, J. K. Norskov, J. A. Dumesic, *J. Chem. Phys.* **2001**, *114*, 4663-4668.
- [13] R. M. Watwe, B. E. Spiewak, R. D. Cortright, R. D. J. A. Dumesic, *J. Catal.* **1998**, *180*, 184-193.
- [14] A. T. Anghel, S. J. Jenkins, D. J. Wales, D. A. King, *J. Phys. Chem. B* **2006**, *110*, 4147-4156.
- [15] A. T. Anghel, D. J. Wales, S. J. Jenkins, D. A. King, *Chem. Phys. Lett.* **2005**, *413*, 289-293.
- [16] A. T. Anghel, D. J. Wales, S. J. Jenkins, D. A. King, *J. Chem. Phys.* **2007**, *126*, 44710.
- [17] Z. J. Zhao, L. V. Moskaleva, H. A. Aleksandrov, D. Basaran, N. Rosch, *J. Phys. Chem. C* **2010**, *114*, 12190-12201.
- [18] Y. Chen, D. G. Vlachos, *J. Phys. Chem. C* **2010**, *114*, 4973-4982.
- [19] X. Q. Lu, L. Liu, Y. Li, W. Y. Guo, L. M. Zhao, H. H. Shan, *Phys. Chem. Chem. Phys.* **2012**, *14*, 5642-5650.
- [20] R. M. Watwe, R. D. Cortright, J. K. Norskov, J. A. Dumesic, *J. Phys. Chem. B* **2000**, *104*, 2299-2310.
- [21] Z. M. Peng, F. Somodi, S. Helveg, C. Kisielowski, P. Specht, A.T. Bell, *J. Catal.* **2012**, *286*, 22-29.
- [22] B. K. Vu, M. B. Song, I. Y. Ahn, Y. W. Suh, D. J. Suh, J. S. Kim, E. W. Shin, *J. Ind. Eng. Chem.* **2011**, *17*, 71-76.
- [23] R. Burch, L. A. Garla, *J. Catal.* **1981**, *71* (2), 360-372.

- [24] J. Y. Shen, J. M. Hill, R. M. Watwe, B. E. Spiewak, J. A. Dumesic, *J. Phys. Chem. B* **1999**, *103*, 3923-3934.
- [25] V. Galvita, G. Siddiqi, P. P. Sun, A. T. Bell, *J. Catal.* **2010**, *271*, 209-219.
- [26] O. A. Barias, A. Holmen, E. A. Blekkan, *J. Catal.* **1996**, *158*, 1-12.
- [27] F. Delbecq, P. Sautet, *J. Catal.* **2003**, *220*, 115-126.
- [28] M. S. Kumar, D. Chen, A. Holmen, J. C. Walmsley, *Catal. Today* **2009**, *142*, 17-23.
- [29] F. Vigne, J. Haubrich, D. Loffreda, P. Sautet, F. Delbecq, *J. Catal.* **2010**, *275*, 129-139.
- [30] J. Wu, Z. M. Peng, P. P. Sun, A. T. Bell, *Appl. Catal. A-General* **2014**, *470*, 208-214.
- [31] A. W. Hauser, J. Gomes, M. Bajdich, M. Head-Gordon, A. T. Bell, *Phys. Chem. Chem. Phys.* **2013**, *15*, 20727-20734.
- [32] J. Lu, B. Fu, M. C. Kung, G. Xiao, J. W. Elam, H. H. Kung, P. C. Stair, *Science* **2012**, *335*, 1205-1208.
- [33] H. Feng, J. Lu, P. C. Stair, J. W. Elam, *Catal. Letters* **2011**, *141*, 512-517.
- [34] E. Baktash, P. Littlewood, R. Schomacker, A. Thomas, P. C. Stair, *Appl. Catal. B Environ.* **2015**, *179*, 122-127.
- [35] B. J. O'Neill, D. H. K. Jackson, A. J. Crisci, C. A. Farberow, F. Y. Shi, A. C. Alba-Rubio, J. L. Lu, P. J. Dietrich, X. K. Gu, C. L. Marshall, P. C. Stair, J. W. Elam, J. T. Miller, F. H. Ribeiro, P. M. Voyles, J. Greeley, M. Mavrikakis, J. A. Dumesic, *Angew. Chemie Int. Ed.* **2013**, *52*, 13808-13812.
- [36] G. Kresse, J. Furthmuller, *J. Phys. Rev. B* **1996**, *54*, 11169-11186.
- [37] G. Kresse, J. Furthmuller, *J. Comput. Mater. Sci.* **1996**, *6*, 15-50.
- [38] P. E. Blochl, *Phys. Rev. B* **1994**, *50*, 17953-17979.
- [39] G. Kresse, D. Joubert, *Phys. Rev. B* **1999**, *59*, 1758-1775.
- [40] J. P. Perdew, Y. Wang, *Phys. Rev. B* **1992**, *45*, 13244-13249.
- [41] H. J. Monkhorst, J. D. Pack, *Phys. Rev. B* **1976**, *13*, 5188-5192.
- [42] G. Henkelman, B. P. Uberuaga, H. J. Jonsson, *J. Chem. Phys.* **2000**, *113*, 9901-9904.
- [43] J. Greeley, M. Mavrikakis, *Surf. Sci.* **2003**, *540*, 215-229.
- [44] Y. Zhang, J. Y. Yu, Y.-H. Yeh, R. J. Gorte, S. Rangarajan, M. Mavrikakis, *J. Phys. Chem. C* **2015**, *119*, 28970-28978.
- [45] S. M. George, *Chem. Rev.* **2010**, *110*, 111-131.
- [46] R. L. Puurunen, *J. Appl. Phys.* **2005**, *97*, 121301.
- [47] M. K. Wiedmann, D. H. K. Jackson, Y. J. Pagan-Torres, E. Cho, J. A. Dumesic, T. F. Kuech, *J. Vac. Sci. Technol. A* **2012**, *30* (1), 01A134.

- [48] D. W. Flaherty, D. D. Hibbitts, E. I. Gurbuz, E. Iglesia, *J. Catal.* **2014**, *311*, 350-356.
- [49] C. T. Campbell, J. R. V. Sellers, *J. Am. Chem. Soc.* **2012**, *134*, 18109-18115.
- [50] K. Reuter, M. Scheffler, *Phys. Rev. B* **2001**, *65*, 35406.
- [51] B. Meyer, *Phys. Rev. B* **2004**, *69*, 45416.
- [52] G. Kresse, O. Dulub, U. Diebold, *Phys. Rev. B* **2003**, *68*, 245409.
- [53] J. Barbier, *Appl. Catal.* **1986**, *23*, 225-243.
- [54] M. Guisnet, P. Magnoux, *Appl. Catal. A-General* **2001**, *212*, 83-96.
- [55] M. M. Bhasin, J. H. McCain, B. V. Vora, T. Imai, P. R. Pujado, *Appl. Catal. A-General* **2001**, *221*, 397-419.
- [56] R. D. Cortright, J. M. Hill, J. A. Dumesic, *Catal. Today* **2000**, *55*, 213-223.
- [57] P. Biloen, J. N. Helle, H. Verbeek, F. M. Dautzenberg, W. M. H. Sachtler, *J. Catal.* **1980**, *63*, 112-118.
- [58] R. D. Cortright, J. A. Dumesic, *J. Catal.* **1994**, *148*, 771-778.

Table of Contents Entry



Atomic layer deposition (ALD) alumina overcoating over Pt enhances ethylene production and decreases coke formation in ethane dehydrogenation.